Obstacle-induced perturbations on turbulent quantities measured in airflows over the sea

S. FERRARESE ([1]), P. BACCI ([4]), D. BERTONI ([1]), C. CASSARDO ([2]), R. FORZA ([1])
C. GIRAUD ([3]), A. LONGHETTO ([1]), M. G. MORSELLI ([4]), M. PANGIA ([5]) and R. PURINI ([5])

([1]) *Dipartimento di Fisica Generale, Università di Torino - Torino, Italy*
([2]) *DSTA, Università di Torino, Sede di Alessandria - Alessandria, Italy*
([3]) *Istituto di Cosmogeofisica, CNR - Torino, Italy*
([4]) *Centro Ricerche Ambiente e Materiali (CRAM) - Milano, Italy*
([5]) *Istituto Talassografico, CNR - Trieste, Italy*

(ricevuto il 5 Marzo 1997; revisonato il 5 Novembre 1997, approvato il 15 Novembre 1997)

Summary. — An experimental campaign, aiming to investigate the perturbation effects induced by fixed obstacles on turbulence measurements in airflows at the air-sea interface, was carried out at the marine platform of the Italian Navy, located in the harbour of La Spezia (North Ligurian Sea, Italy), near Lerici, on 28th, 29th, and 30th June 1994. This study was prompted by the ever-growing interest in more reliable estimates of energy, mass, and momentum exchanges between water surfaces and atmosphere, whose measurements are severely limited by the geometrical constraints of floating or fixed platforms where they are installed. Two types of meteorological instruments have been used: fast response (20 and 21 Hz) ultrasonic anemometers and fluxmeters to measure turbulent momentum, sensible, and latent heat fluxes and slow-response sensors (less than 4 Hz and sampled at a rate of 10^{-2} Hz) to measure average wind and temperature vertical profiles in the perturbed boundary layer. Both fast- and slow-response instruments have been located a few meters apart from each other, along horizontal and vertical directions, so as to establish also an upper limit to the reliability of horizontal and vertical divergences and gradients of average and turbulent quantities in the obstacle wake. It has been observed that, in the airflow perturbed by the marine platform and its fixed structures, the fast-response instruments of the same type and made by the same manufacturers gave results that compared well with each other, even if they were located at different positions and heights (except for the vertical component of turbulent wind speed), while the comparison among different types of fast instruments gave more uncertain results. On the contrary, as far as mean values of the physical quantities were concerned, the measurements of slow-response instruments in the perturbed airflow were always in good agreement with the averaged data of fast instruments, irrespective of their factory or construction features.

PACS 92.60.Ek – Convection, turbulence, and diffusion.
PACS 92.10.Kp – Sea-air energy exchange processes.
PACS 92.60.Fm – Boundary layer structure and processes.

1. – Introduction

Exchanges of energy, mass, and momentum across water surfaces (oceans, seas and lakes) all over the Earth, influence atmospheric and oceanic circulation over a whole spectrum of time and spatial scales [1-6]. Therefore, it is important to evaluate the energy budget near the air-water interface and many efforts have been made to organize complex and over-refined experiments to fill the gaps still existing in the comprehension of these processes. Momentum, sensible- and latent-heat flux have been usually estimated by using bulk aerodynamic formulae and flux-gradient relationships. These methods require the measurement of wind, temperature, and humidity profiles, which are usually taken from ship- or platform-based soundings carried out with pilot balloons, radiosondes, minisondes and more sophisticated profilers. As data for calibrating the above-mentioned relationships are inadequate, mainly in low wind conditions, so that it becomes difficult to determine the various coefficients and functions appearing in the formulae [7], serious problems can arise in the calculation of turbulent fluxes. For this reason, the direct method based on the correlated products of directly measured turbulent quantities is often preferred, also with the purpose of improving the determination of the empirical coefficient of the bulk formulae. This method requires the deployment of fast-response systems near the air-waterinterface.

In general, however, the energy budget obtained from data taken in the atmospheric boundary layer (over the sea as well as over the ground) can be complicated by:

– the use of instruments manufactured by different factories: systematic errors might be introduced in the evaluation of any turbulent quantity as well as of its vertical profile in the ABL;

– the surface inhomogeneities (roughness, temperature, wetness, or elevation [8]), on account of their important effects on the atmospheric flows;

– the non-steadiness of meteorological conditions;

– the sounding systems, that can only provide instantaneous or inadequately averaged winds and other meteorological variables, which generally deviate from and scatter around the expected mean profiles of these variables.

These complexities are enhanced over water surfaces, where a reliable evaluation of various terms occurring in the energy budget from measured quantities is made more problematic by the border effects, on the impinging air-flow, played by the abrupt discontinuity represented by the complex and massive structures of platforms and masts over an otherwhise flat and extended fetch of water. This not only perturbs turbulent quantities measured at the same level, but also makes indefinite the depth of inner layers and the lower limit of the unperturbed outer layer.

This paper describes the measurement campaign, carried out near Lerici (La Spezia, Italy) on June 28-30, 1994, with the aim to test the instruments that are currently used in studies concerning the air-sea interaction and compare the performances of fast-response instruments, deployed for studying energy balances at the air-sea interface, under disturbed airflow conditions.

Many instruments, operating according to different working principles and sampling frequencies (*i.e.* fast- and slow-response sensors) and to distinctive construction features (for example, the Solent and Kaijo Denki ultrasonic anemometers) have been used.

2. – Experimental layout and instrument description

Instruments were set up on a fixed concrete platform owned by the Italian Navy and built inside the artificial breakwater that protects from rough sea the Port of La Spezia (fig. 1a).

TABLE I. – *List of instrumentation used their characteristics and location.*

	Height (a.s.l.)	Length	Width	Orientation	Separation
Breakwater	2.5 m	2.5 km	5 m	70–230 degrees	20 m maximum
Platform	2.5 m	8 m	6 m	90–270 degrees	25 m maximum

Fast-response sensors

Sensor	Sampling height a.s.l.	Sampling frequence	Variables	Sampling range	Manufacturer	Model
SONIC1	4 m	21 Hz	u, v, w, C	0.26–60 m/s	Gill Instruments	Research-asymmetric
SONIC2	4 m	21 Hz	u, v, w, C	0.26–60 m/s	Gill Instruments	Research-symmetric
SONIC3	10 m	21 Hz	u, v, w, C	0.26–60 m/s	Gill Instruments	Research-symmetric
SONANA	4 m	21 Hz	u, v, w, C	0.26–60 m/s	Gill Instruments	Research-symmetric
Kaijo Denki	10 m	20 Hz	u, v, w, T_s	0.2–30 m/s	Kaijo Denki	Dat - 300
Sensible heat	4 m	21 Hz	w, t	2.2–30 m/s −20–40 °C	Campbell	CA 27 (w) 127 (T)

Slow-response sensors

Sensor	Sampling height (a.s.l.)	Sampling frequency	Variables	Sampling range	Manufacturer
SITEP1	5 m	4 Hz	speed (±0.5 m/s) dir (±3°)	speed (0.5–60 m/s) dir (0–360°)	SITEP
TEMP1	5 m	10^{-2} Hz	T(°C)	−30–70 °C	SITEP
rh1	5 m	10^{-2} Hz	rh (%)	0–100 %	SITEP
SITEP2	7.5 m	4 Hz	speed (±0.5 m/s) dir (±3°)	speed (0.5–60 m/s) dir (0–360°)	SITEP
TEMP2	7.5 m	10^{-2} Hz	T(°C)	−30–70 °C	SITEP
rh2	7.5 m	10^{-2} Hz	rh (%)	0–100 %	SITEP
SITEP3	10 m	4 Hz	speed (±0.5 m/s) dir (±3°)	speed (0.5–60 m/s) dir (0–360°)	SITEP
TEMP3	10 m	10^{-2} Hz	T(°C)	−30–70 °C	SITEP
rh3	10 m	10^{-2} Hz	rh (%)	0–100 %	SITEP
Barometer	2.5 m	10^{-2} Hz	p(±1 hPa)	800–1100 hPa	SITEP
Solarimeter	2.5 m	10^{-2} Hz	Glob. Rad (±1.5 W/m^2)	0–1500 W/m^2	SITEP

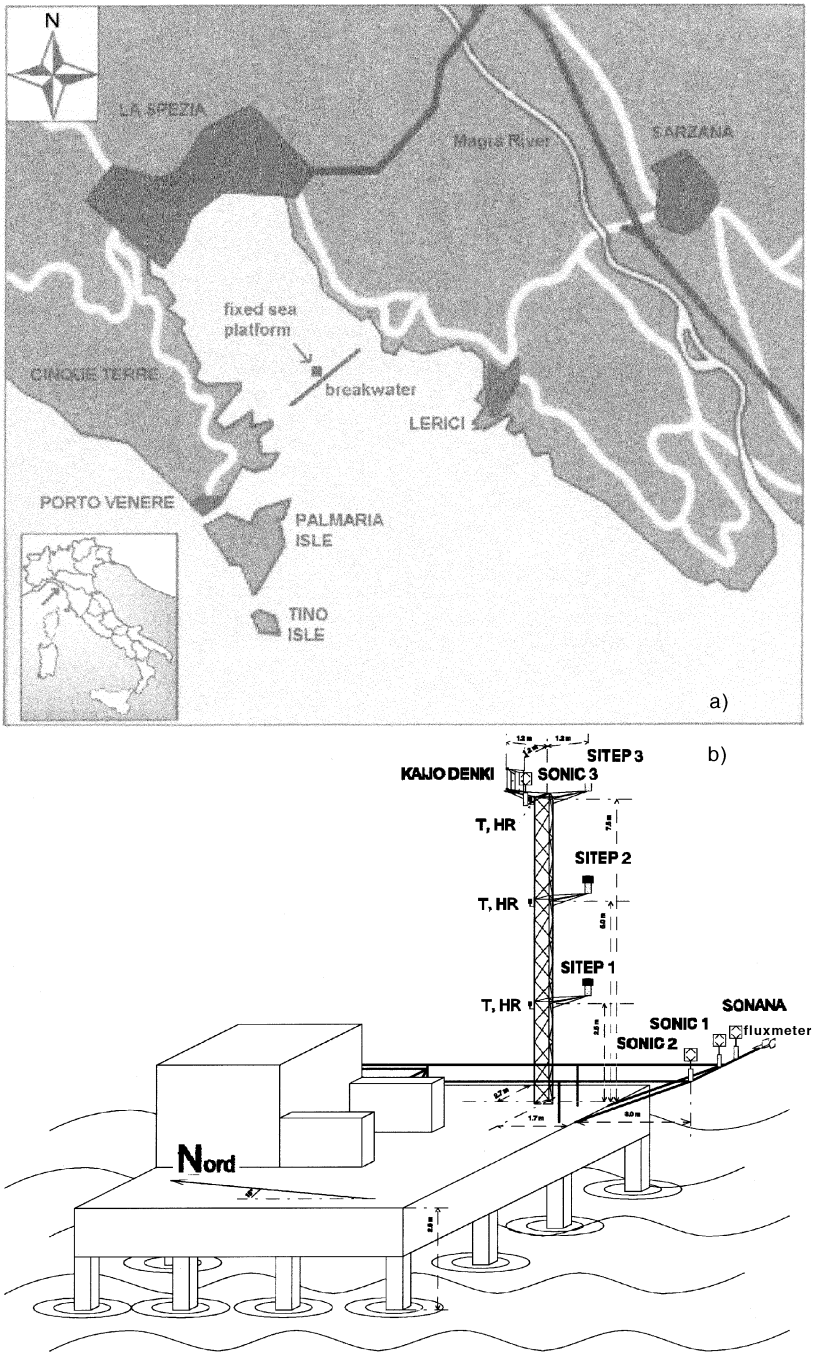

Fig. 1. – a) Map of La Spezia Gulf, showing the location of the sea platform. b) View of the platform and instrumentation layout.

This sampling site, even if located in a region of still and shallow sea near the coast, nevertheless offered a good opportunity to study the perturbation induced by the structure of a squared massive body and an elongated breakwater on the airflow interacting with the underlying water surface and on turbulent energy and mass fluxes at the air-sea interface.

To get a global view of the experimental set-up, we have resumed in table I all the instrumentation used, their characteristics, their locations on the mast and the booms, and their height over the sea.

The instrument set was formed by six instruments working at high sampling rate (a Campbell sensible-heat fluxmeter, made up by one vertical sonic anemometer and one fast sensor for air temperature, and five ultrasonic anemometers: four of them, Solent, manufactured by Gill and one by Kaijo Denki), and by a dozen of low-frequency instruments (a barometer, a solarimeter, four thermometers, three hygrometers and three anemometers). The sampling frequency was equal to 21 Hz for the Solent anemometers and for the fluxmeter and to 20 Hz for the Kaijo Denki anemometer; for all other instruments, on the contrary, the sampling rate was 10^{-2} Hz, with the exception of Sitep anemometers whose sampling rate was 4 Hz.

Each instrument was arranged over the measuring site as follows (see fig. 1b):

– the solarimeter and the barometer were installed directly on the platform at 2.5 m a.s.l.

– the sensible-heat fluxmeter and the 3 Solent anemometers, 2 of them constructed in symmetric version and 1 in asymmetric version (hereafter named SONIC2, SONANA and SONIC1, respectively), were set up over the sea at the extremity of booms at about 4 m a.s.l. The two sonic anemometer versions (symmetric and asymmetric) are different for the arrangement of the three supportive arms of the trasducers, that are symmetric to the central axis in the symmetric version and asymmetric in the other one;

– one symmetric Solent anemometer, named SONIC3, one Kaijo Denki anemometer, a thermometer, a hygrometer and an anemometer were set up at 10 m a.s.l. on a tower built on the platform, while two thermometers, two hygrometers and two anemometers were installed at 7.5 m and 5 m a.s.l., respectively, on the same tower;

– finally, one temperature sensor was fitted up under water, at 1 m b.s.l.

The detailed descriptions of the instrumental features of the sensors deployed in this experiment are reported in appendix A).

The campaign started at about 2 p.m. on June, 28th, 1994 and ended at about 9 a.m. on June, 30th, 1994, with approximately 43 hours of sampling.

3. – Data handling

Data recorded by the ultrasonic anemometers have been processed through the SONELA model [9]. According to this algorithm, three consecutive rotations [10] are imposed to the reference frame:

a) the x co-ordinate of the reference system is aligned with the mean horizontal wind ($\overline{v} = 0$), and the rotation angle α between the mean-horizontal-wind direction and the North direction is then computed;

b) the x co-ordinate of the reference system is aligned with the mean 3D wind vector ($\overline{w} = 0$), and the angles α and δ are then calculated;

c) a rotation around the x-axis is performed, to ensure that $\overline{v'w'} = 0$, the angle ψ is then calculated.

These numerical operations make the anemometer set up with its x-axis along the streamlines. Aligning the instrument in a streamline system is necessary to avoid the serious errors which may occur in the calculations of turbulent fluxes if the wind sensor is not vertical (misalignment problem) or if the mean streamline is not perfectly horizontal, this last condition generally occurring in complex or irregular terrain as well as in case of obstruction brought about by other sensors.

Our sofware allows to compute a set of 30′ averaged quantities evaluated after the 3 rotations such as horizontal wind speeds, sonic temperatures and their standard deviations, wind directions, rotation angles (α, δ and ψ), and the second-order crossed statistical moments of the fluctuating quantities, including momentum, sensible- and latent-heat fluxes [9, 11].

The values of mean vertical velocity, calculated before the rotation, are also shown by the software in order to provide an idea of its magnitude before the correction of misalignment. As to the sensible heat flux, it is necessary to specify that the ultrasonic anemometer strictly allows the evaluation of the so-called "sonic" sensible-heat fluxes, which can be computed by using the relation: $H_0 = \varrho c_p \overline{T_s' w'}$, where ϱ is the air density, $c_p = 1004.67\ \mathrm{J/K\,kg}$ T_s' is the sonic temperature fluctuation and w' represents the vertical velocity fluctuation; on the contrary, with the fluxmeter, where the absolute temperature fluctuations are available, it is possible to calculate the "true" sensible heat flux $H_0 = \varrho c_p \overline{T'w'}$).

The "sonic" temperatures measured by sonic anemometers have been compared with those computable from traditional instruments' data through the relation: $T_s = T(1 + 0.529q)$ The specific humidity q is derived from pressure, temperature and relative-humidity data according to the formula: $q = 0.622e/(p - 0.378e)$, where p is the pressure measured by the barometer and e is the vapour partial pressure. The values of e have been derived in this way: $e = (u/100)\, e^*$, with u indicating the relative humidity measured by hygrometers fixed at different heights of the mast and e^* the saturation vapour pressure calculated through the relation: $e^* = 6.1078 \exp[17.269((T - 273.15)/(T - 35.86))]$, [12], with T being the absolute temperature measured by thermometers set up along the mast.

4. – Meteorological situation

Looking at the maps of the EMB (European Meteorological Bulletin) of 27th June 1994 (fig. 2a), we see that a wedge of high pressure (1020 hPa), following a front passage, moved over Northern Italy on 27th and grew at the surface on 28th (fig. 2b) on the Western side of the Po Valley, while at higher levels a cyclonic area, centered on Sardinia, was slowly filling; this low pressure was associated with the front of cold air (constituting the so-called "cold-air drop") and caused unstable weather conditions along the Tyrrhenian coastal regions during the afternoon of 28th, with some showers or thunderstorms as the one experienced at the campaign site. The potential instability of air over Northern Italy can be inferred from the analysis of the Milan radiosounding of 12 UTC of 28th (as well as from EMB—not shown here). They reveal the presence of low- (900 hPa) and middle-level (650 hPa) clouds and the possibility of deep convection

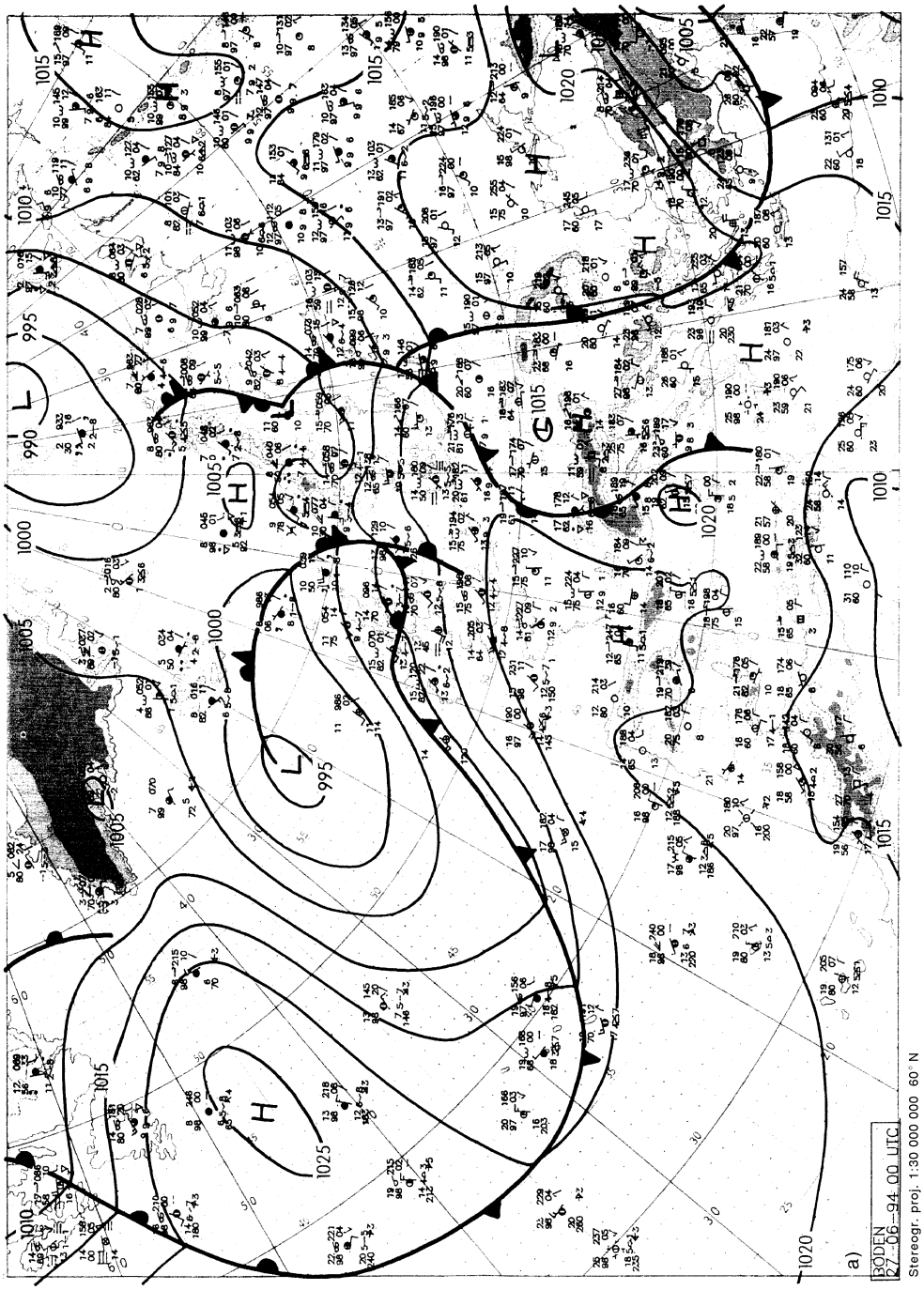

Fig. 2. – Meteorological map of 27th June at 00UTC.

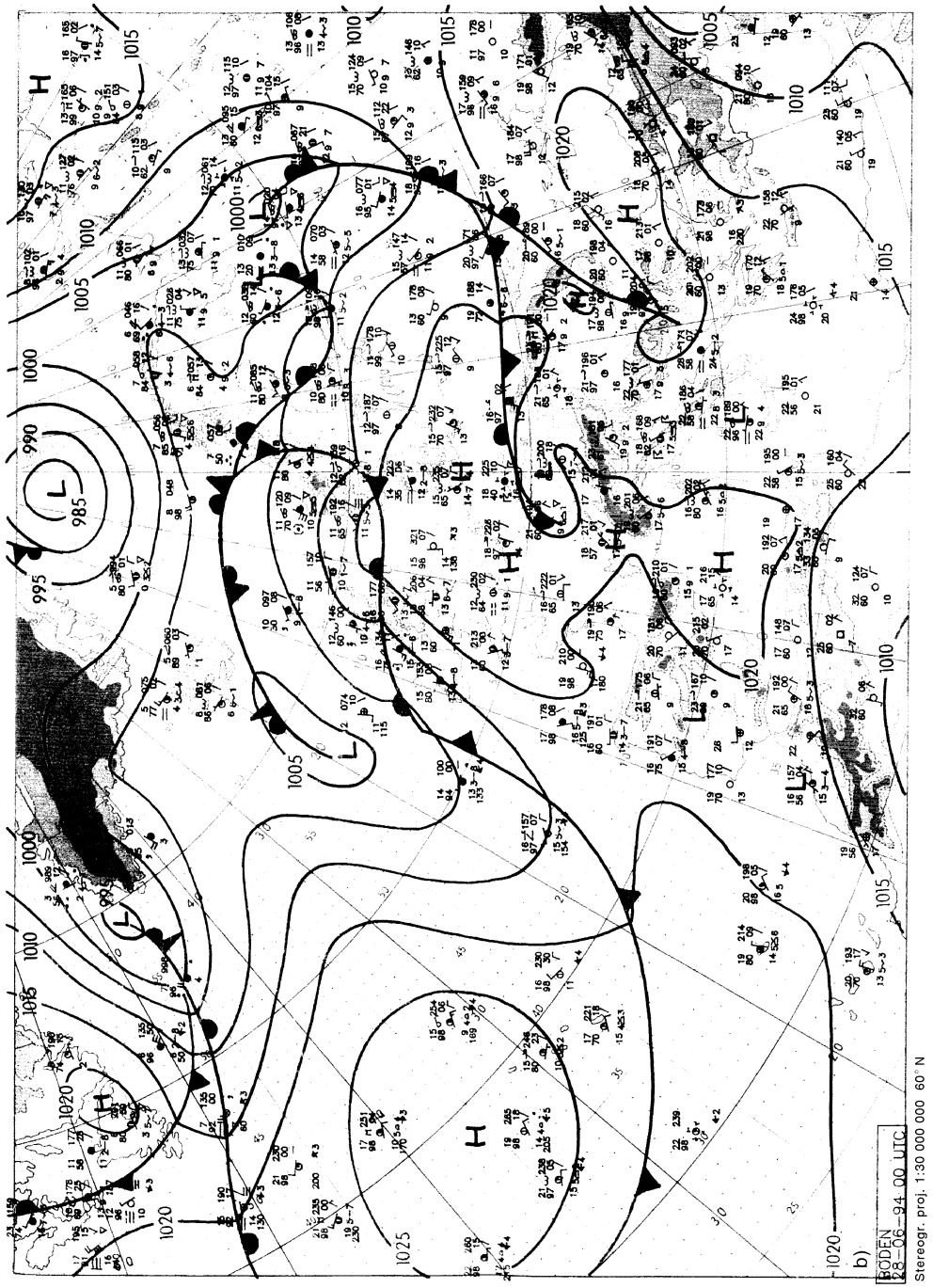

Fig. 2. – Meteorological map of 28th June at 00UTC.

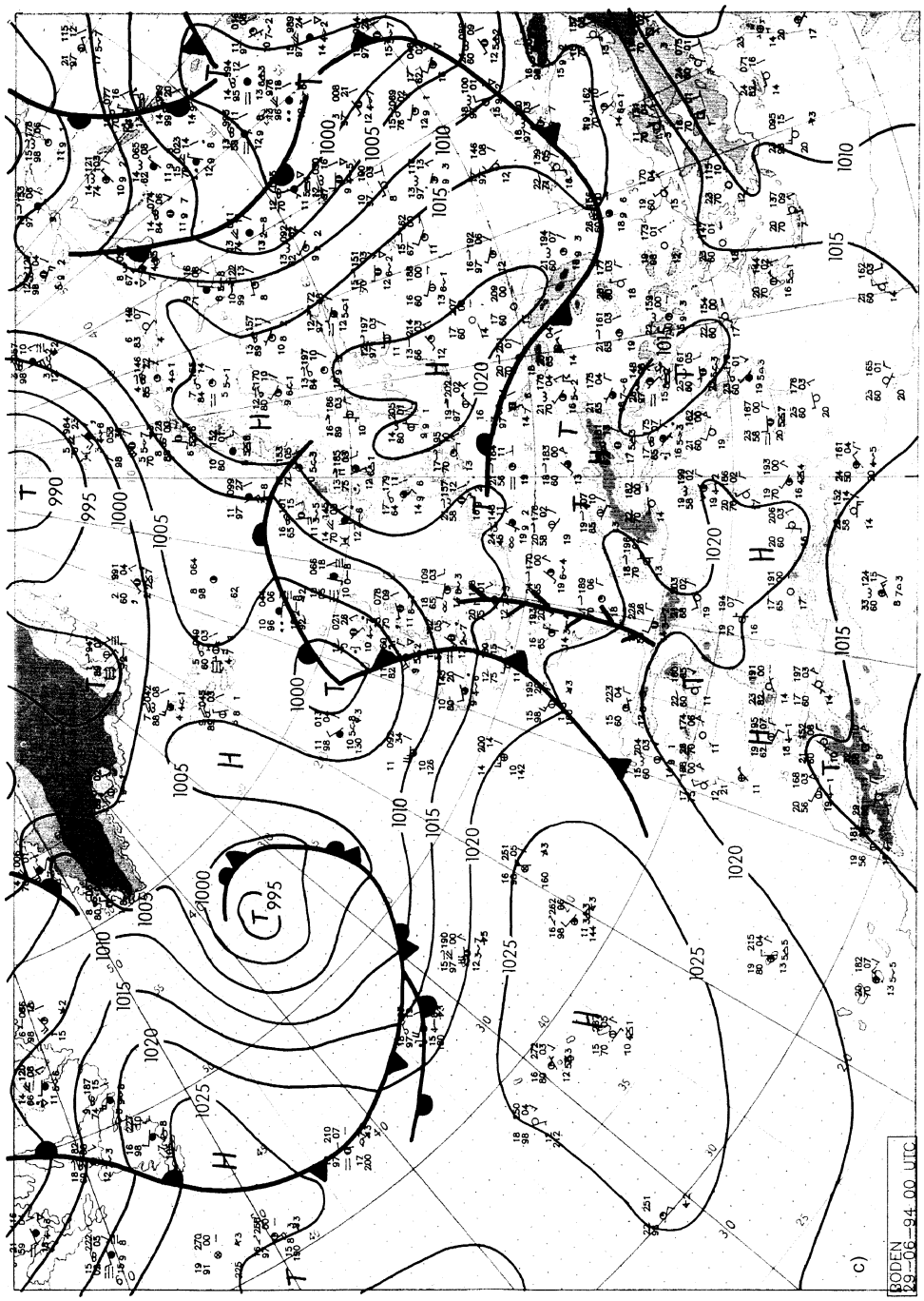

Fig. 2. – Meteorological map of 29th June at 00UTC.

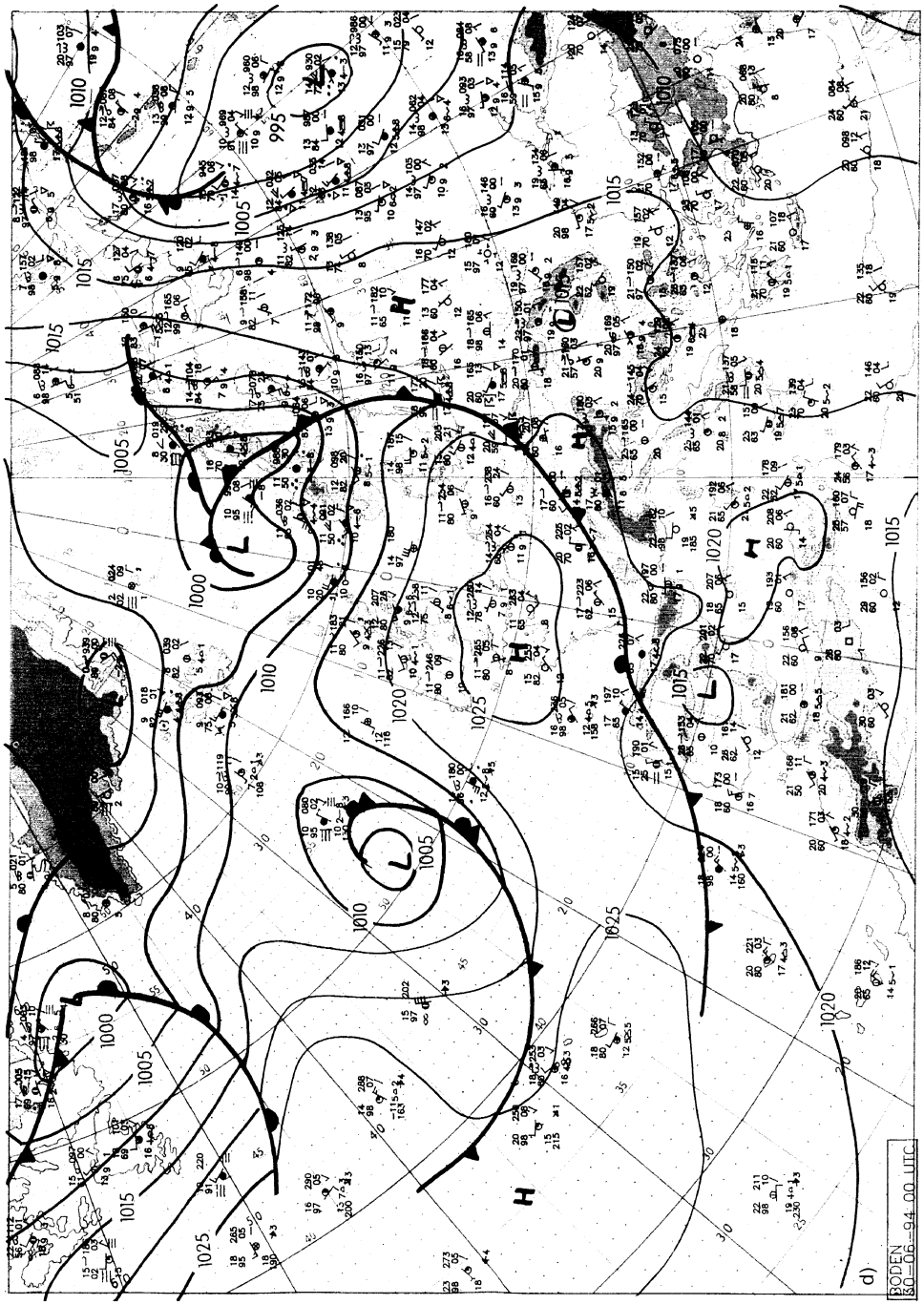

Fig. 2. – Meteorological map of 30th June at 00UTC.

conditionally to a surface temperature exceeding 30 °C. The above-mentioned high-level low-pressure system gradually filled and, on 29th (fig. 2c), it was present only on the 700 hPa surface and centred between Sardinia and Sicily islands. On 29th and 30th (fig. 2d) Northern Italy experienced a relatively fine weather due to the levelling of the high-pressure wedge also at higher levels; this wedge contributed to weaken and to slow the motion of the frontal system on the northern side of the Alps. The air stability in these two days is emphasized by the Milan radiosoundings of 12 UTC in which a little inversion at 550 hPa acts as a lid for the convection beneath and results also from the sudden drop of more than 30 °C in the dewpoint temperature above this level.

5. – Discussion of results

5˙1. *Low-response instruments data.* – As mentioned in sect. **2**, the low-response instruments recorded global radiation, pressure, temperature and relative humidity at different heights. The radiation data (fig. 3) recorded during the three days were quite regular and showed the typical day-night oscillation; the data on 28th afternoon are more scattered because of a strong thunderstorm occurring from 4 p.m. to 7 p.m. (see sect. **4**). The air temperature trends (fig. 4) recorded at different heights (5 m, 7.5 m, 10 m a.s.l.) were very much alike (within the instrument sensitivity), with an absolute minimum at about the end of the night between 28th and 29th and a maximum during the midafternoon of 29th. The sea water temperature at 1 m below sea level (filtered by running average), owing to the higher heat capacity of the water showed a different behaviour, with fluctuations of less than two degrees on a short-period basis and a 24 h oscillation in its trend, due to the day-night cycle, whose amplitude was about 1 °C. Anyway, the time trends of fig. 4 depict a typical thermal stratification of air over the sea, with unstable condition in the lower layers over a warmer sea surface during the

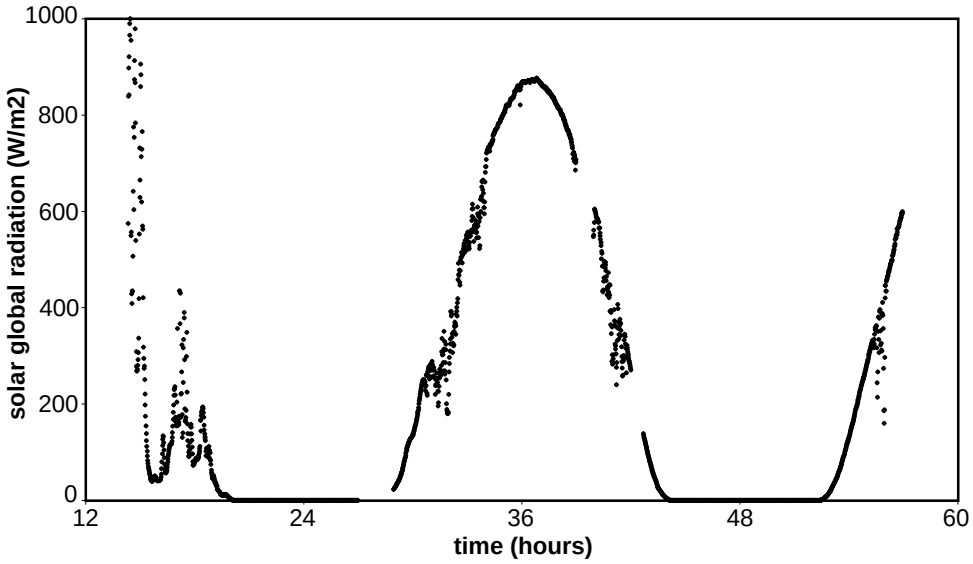

Fig. 3. – Time series of global incoming radiation (W m^{-2}).

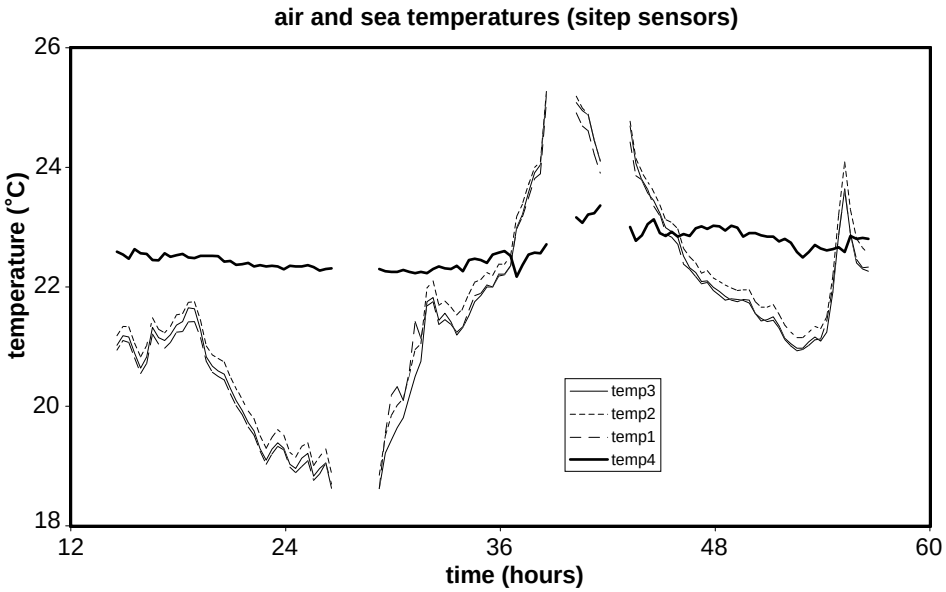

Fig. 4. – Time series of air and sea temperatures (in degrees centigrade) measured, respectively, at 5 m (temp1), 7.5 m (temp2), 10 m a.s.l. (temp3) and 1 m b.s.l. (temp4) by the SITEP sensors.

night and the opposite situations during daytime. The mean pressure (fig. 5, left scale, filtered by running average) remained almost constant during the observation period, its fluctuations being limited to 3 hPa. The hygrometers (fig. 5, right scale) recorded relative-humidity values very much alike between 5 and 10 meters a.s.l.; their minima

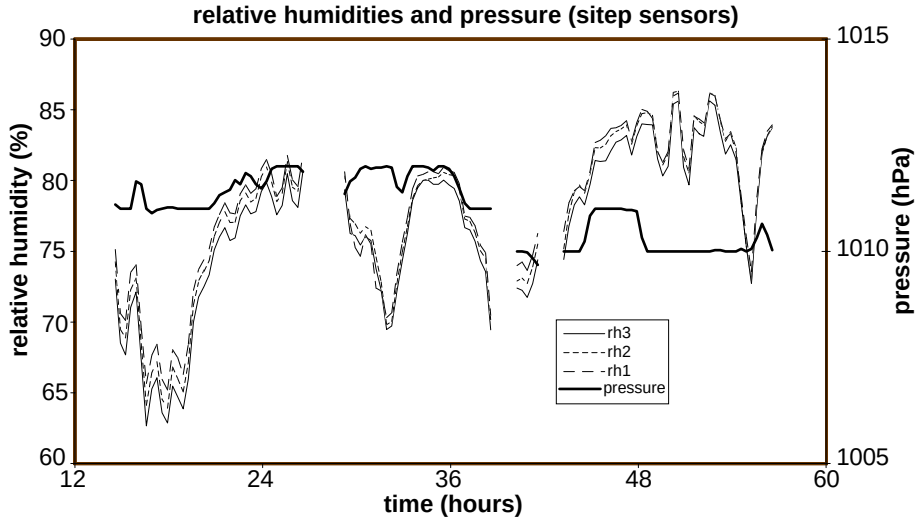

Fig. 5. – Time series of air pressure (hPa) on left scale and time series of relative humidities r (%) measured, respectively, at 5 m (rh1), 7.5 m (rh2) and 10 m a.s.l. (rh3).

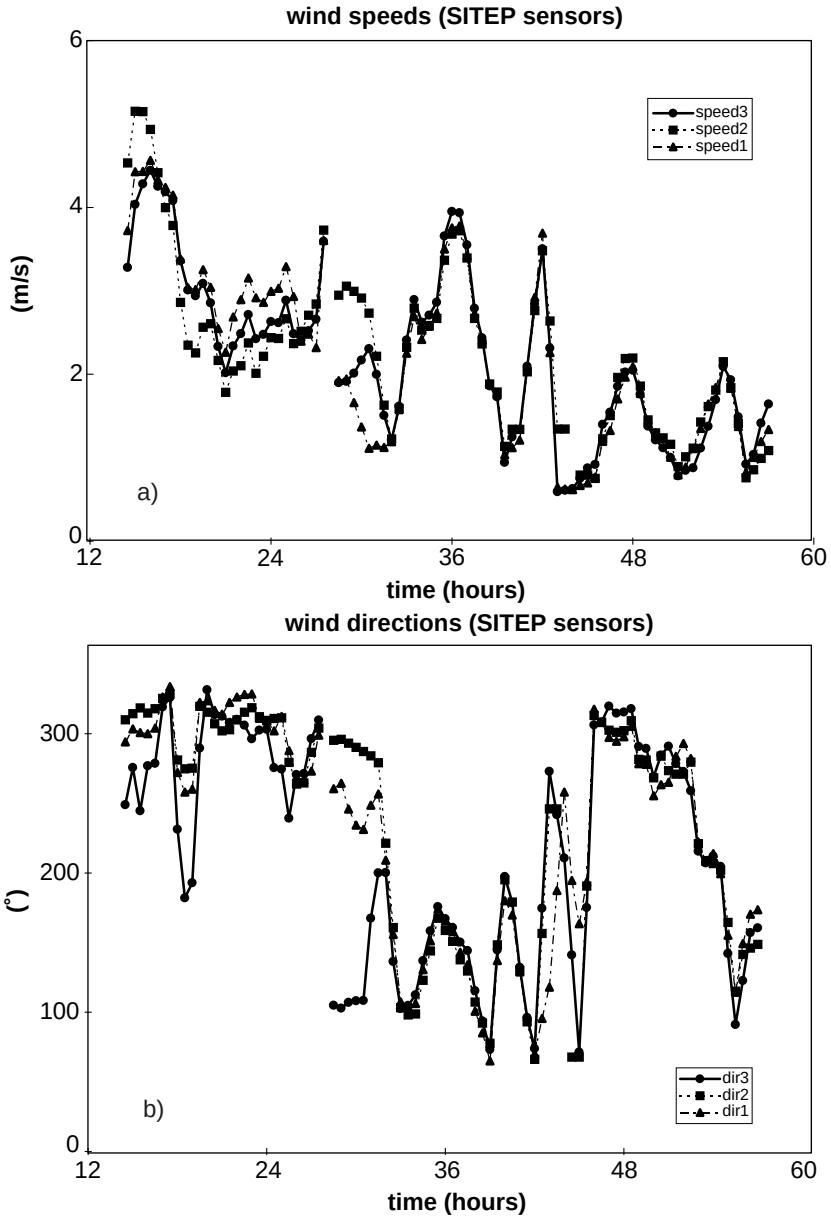

Fig. 6. – a) Horizontal wind speeds measured, respectively, at 5 m (speed1), 7.5 m (speed2) and 10 m a.s.l. (speed3) all in m/s from SITEP anemometers. b) Horizontal wind directions measured, respectively, at 5 m (dir1), 7.5 m (dir2) and 10 m a.s.l. (dir3), all in degrees from SITEP anemometers.

and maxima were anticorrelated with the thermal ones but, owing to the continuous sea evaporation, their signals showed variations lower than 25%. Figures 6a) and b), respectively show time records of 30′ averages of wind speed and direction recorded by

the SITEP anemometers at 5, 7.5 and 10 meters a.s.l. It is possible to observe higher speeds during the first sampling hours (due to the thunderstorm) and a more regular trend in the following hours, with a daytime maximum of 4 m/s at about 12 a.m. of June 29th. The wind exhibited a regular day-night oscillation, blowing

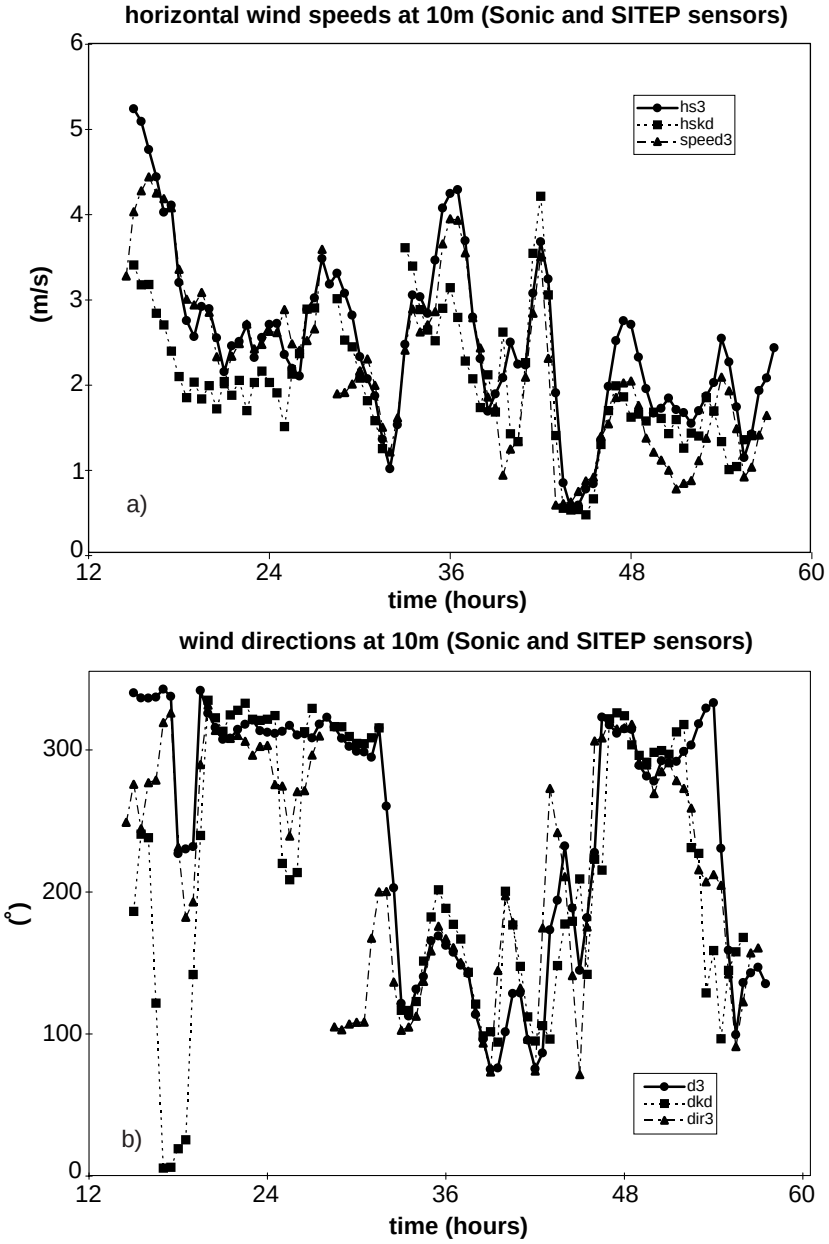

Fig. 7. – a) Horizontal wind speeds measured at 10 m from SONIC3 (hs3), Kaijo Denky (hskd), and SITEP3 (speed3), all in m/s. b) Wind directions measured at 10 m from SONIC3 (d3), Kaijo Denky (dskd) and SITEP3 (dir3), all in degrees.

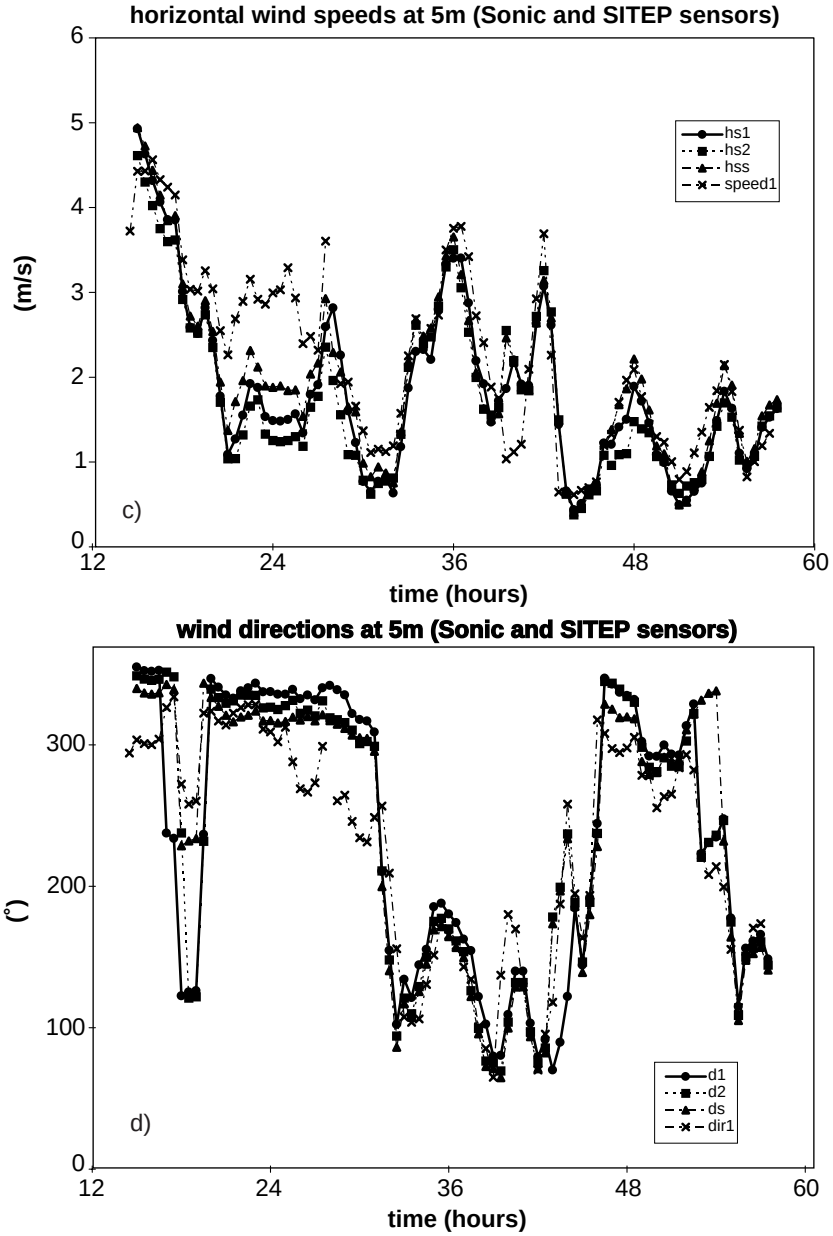

Fig. 7. – c) Horizontal wind speeds measured at 4 m from SONIC1 (hs1), SONIC2 (hs2), SONANA (hss) and at 5 m from SITEP1 (speed1), all in m/s. d) Wind directions measured at 4 m from SONIC1 (d1), SONIC2 (d2), SONANA (ds) and at 5 m from SITEP1 (dir1), all in degrees.

prevalently from NNW (inland) during the night and from ESE (La Spezia Gulf) during the day. Looking at fig. 1b), it seems that shadowing effects of the tower and other instruments could perturb the wind field: more in detail, at 5 and 7.5 m, at least

for the wind blowing from NNW, SITEP1 and SITEP2 were shadowed by the micrometeorological tower. It must be pointed out, however, that flow perturbations were not so relevant, especially in conditions dominated by low winds (fig. 6a) and b)).

5·2. *High-response instrument data.* – In fig. 7 a) to d) time records of horizontal wind speeds and directions recorded by the different fast-response instruments at 4

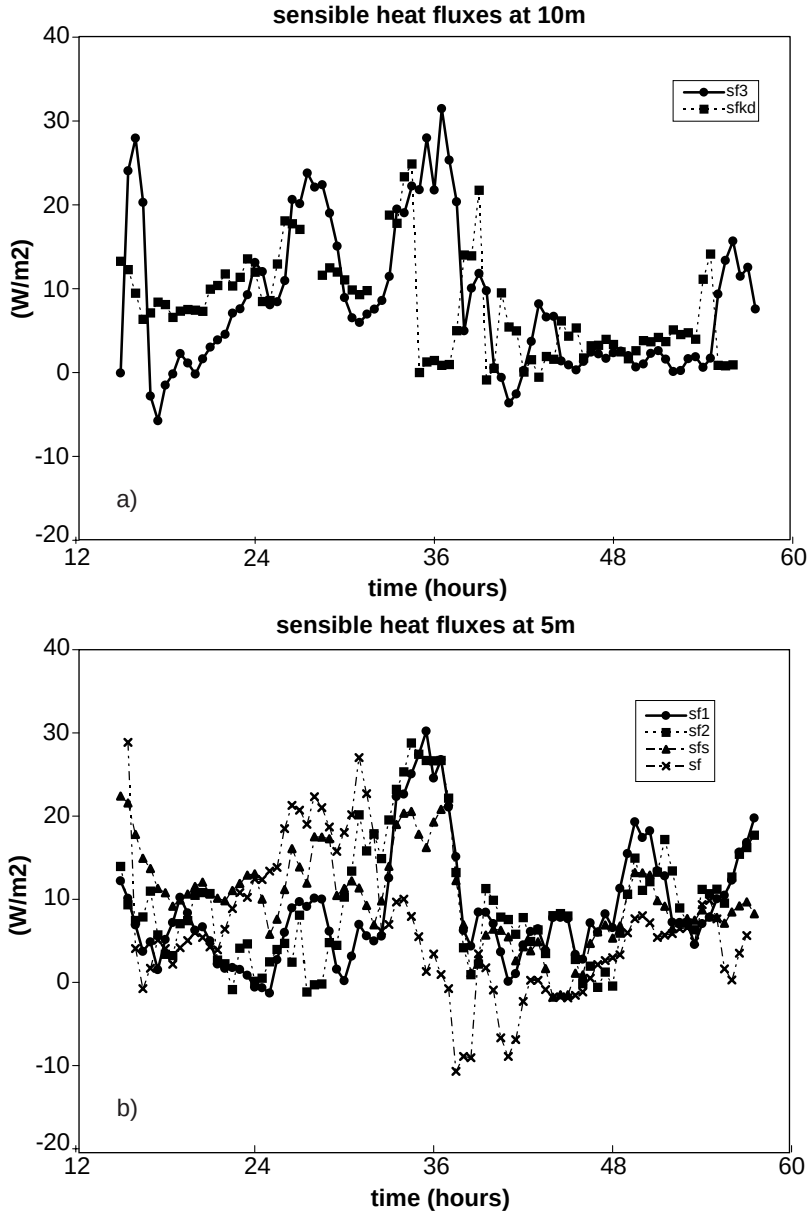

Fig. 8. – a) Sensible-heat fluxes at 10 m calculated from SONIC3 (sf3) and Kaijo Denky (sfkd). b) Sensible-heat fluxes at 4 m calculated from SONIC1 (sf1), SONIC2 (sf2), SONANA (sfs) and fluxmeter (sf).

and 10 m are shown. They are compared with the corresponding wind speed and direction measured at 5 and 10 m by the slow-response SITEP1 and SITEP3 anemometers.

With the exception of a few short periods, an overall good agreement appears for the whole measurement period which is affected by different wind intensity.

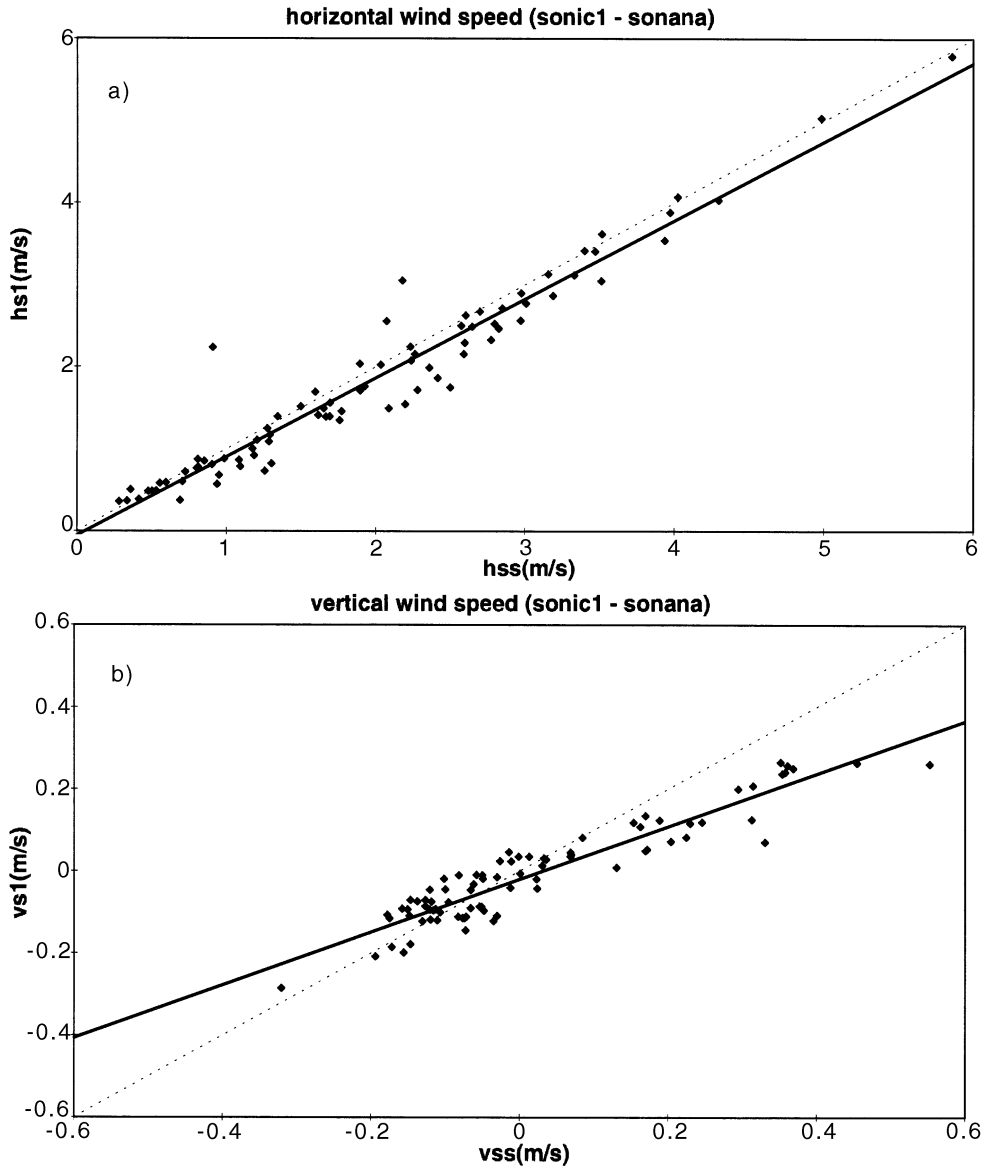

Fig. 9. – SONIC1-SONANA scatter diagrams: hs (a), vs (b), t (c), d (d), u* (e), and sf (f) are, respectively, the horizontal speed, vertical speed, sonic temperature, wind direction, friction velocity and sensible heat flux measured by or calculated from ultrasonic anemometers; 1 and s identify the SONIC1 and SONANA instruments, respectively.

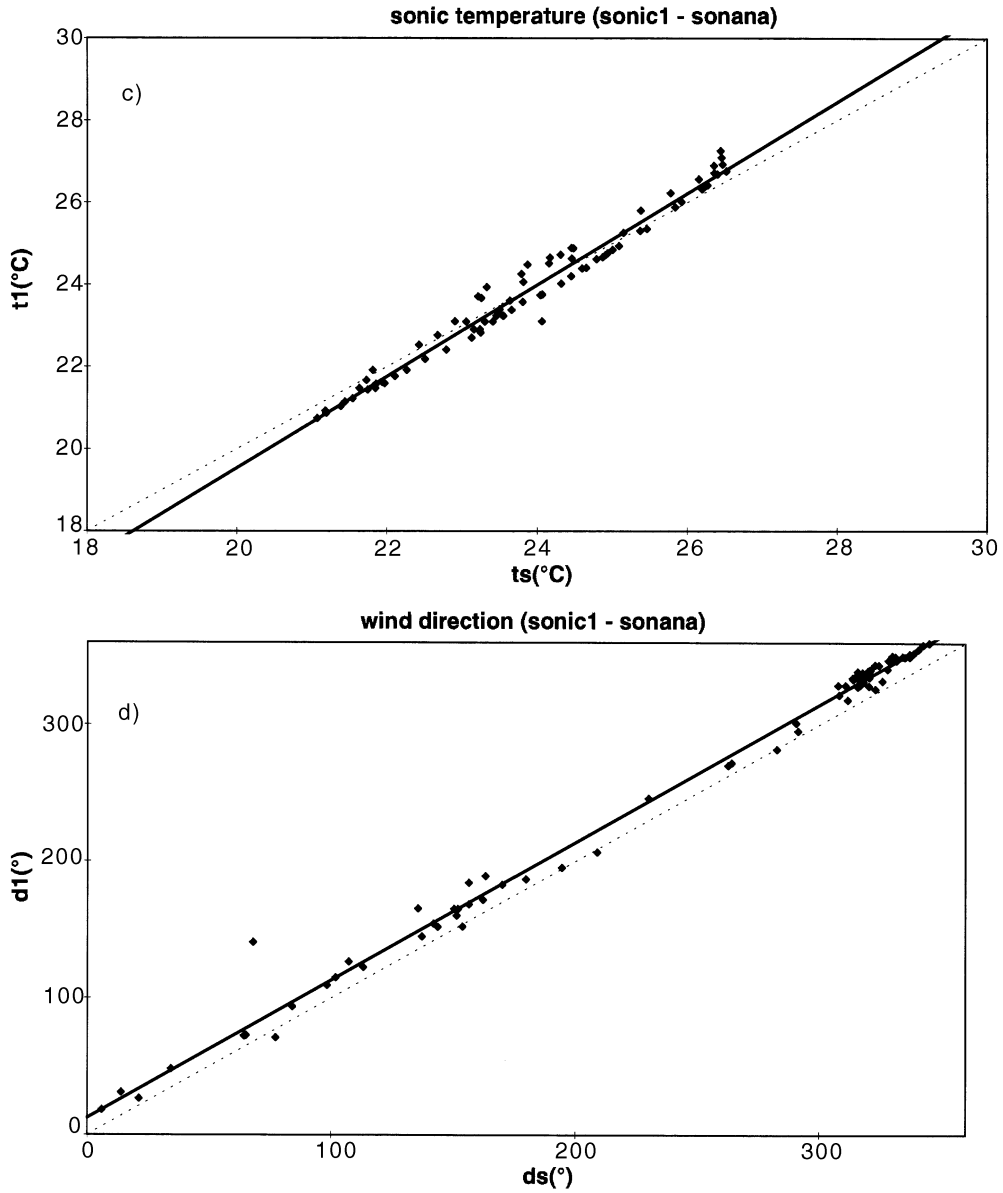

Fig. 9. – *Continued*.

Worthy of remark is that, at 10 m for winds blowing from ESE, SONIC3 could be perturbed by SITEP3, while the comparison of SONIC3 and Kajio Denki time-records (fig. 7a and 7b) clearly shows that larger speed variations sensed by the former correspond to lower changes in wind directions.

This is a quite strange behaviour that deserves some further considerations (for examples, with a laboratory intercalibration experiment under controlled conditions).

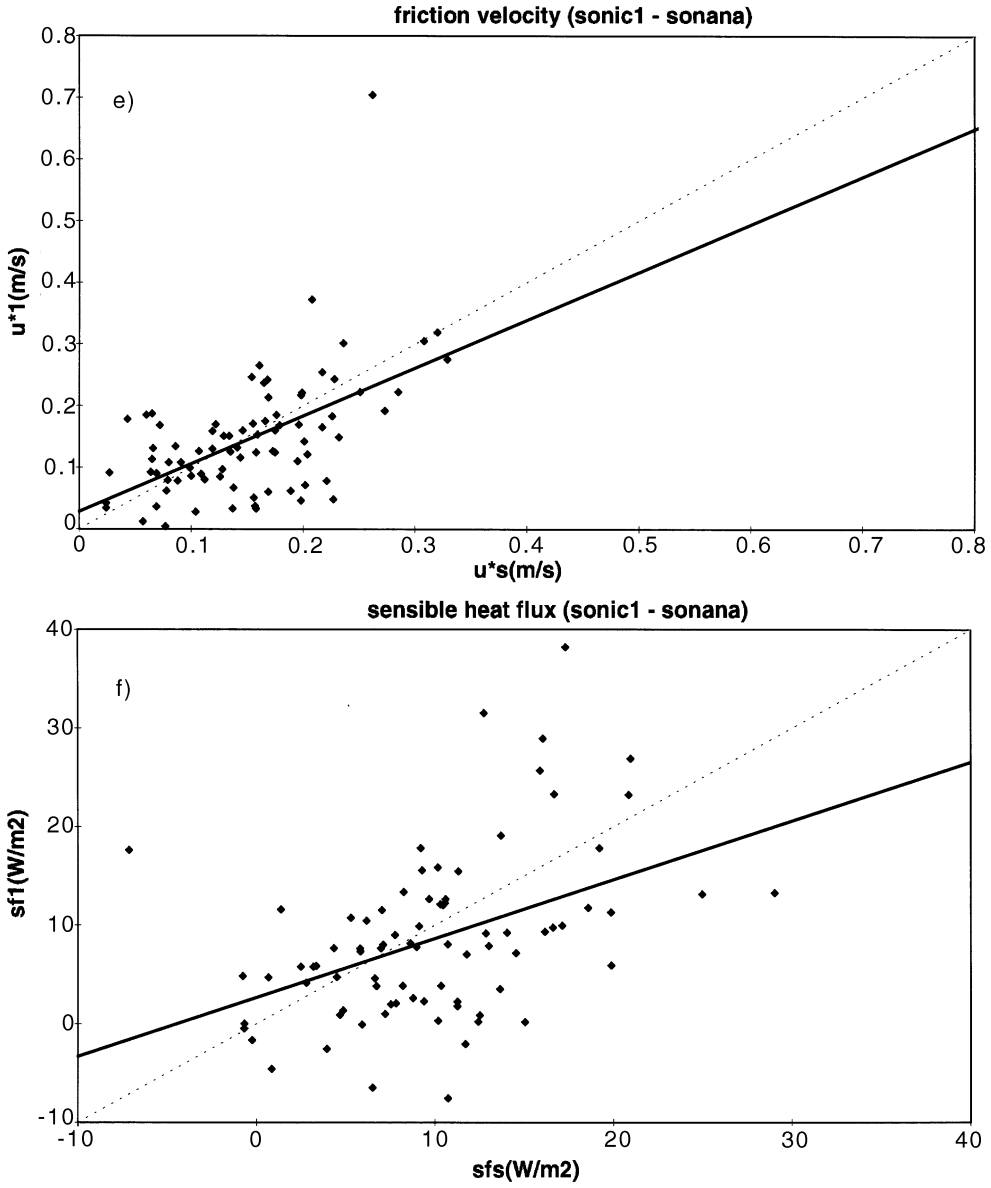

Fig. 9. – *Continued*.

Looking now at the sensible-heat fluxes measured during the field experiment by the different instruments, fig. 8a) and b) show their time trends at 10 m and 4 m.

The values of sensible-heat fluxes appear, on the whole, to be very low, ranging from a maximun of $+30$ W/m^2 during the morning of June 29 to a minimum of -10 W/m^2 in the early afternoon of June 29th (these lower values having been measured by the Campbell sensible-heat fluxmeter).

At both levels the measurements appear to be a little more scattered during the

first half of the observation period, when both higher wind speed and sea surface temperature (with respect to air temperature—see fig. 4) gave rise to more unstable and unsteady conditions, which could also account for the slightly larger values of the flux.

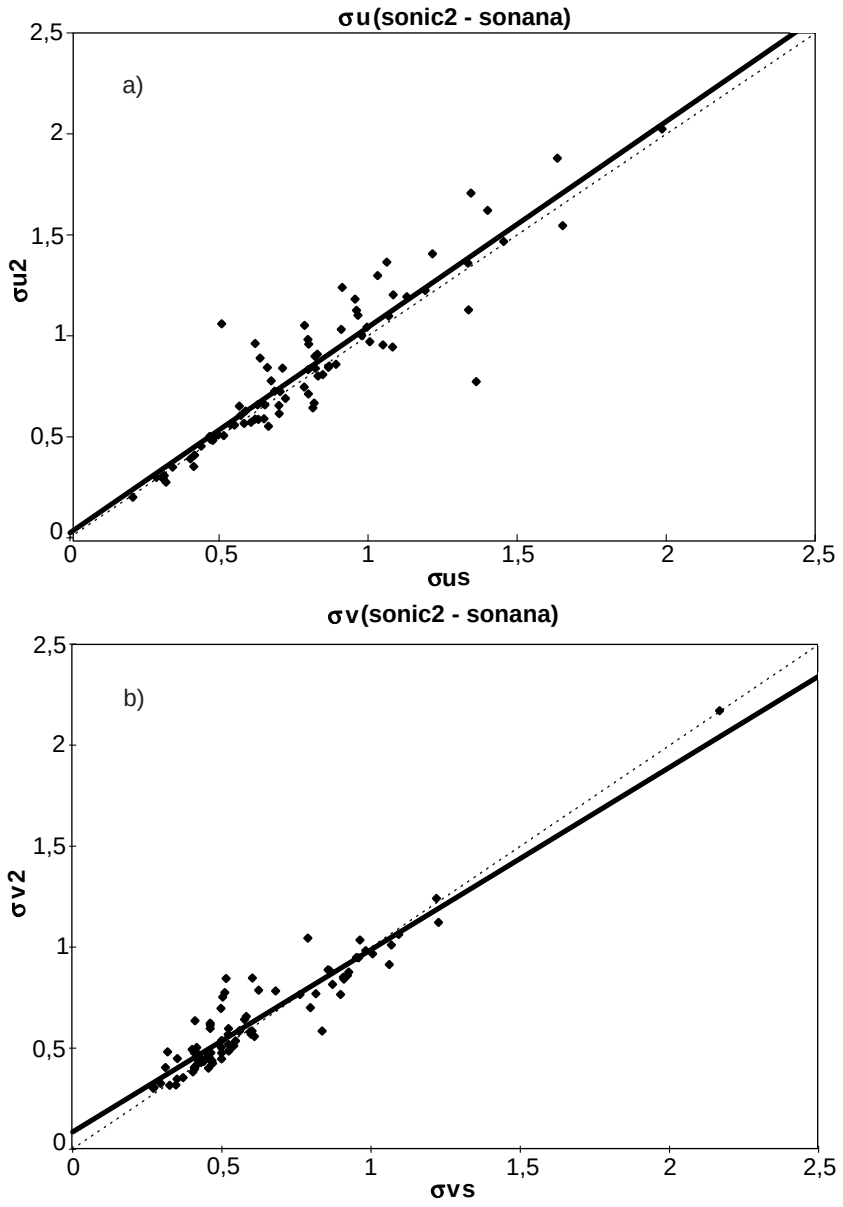

Fig. 10. – SONIC2-SONANA scatter diagrams: σ_u (a), σ_v (b), σ_w (c), σ_t (d) are, respectively, the standard deviations of the two components of horizontal speed (u and v), the vertical speed (w), the sonic temperature (t); δ (e) and ψ (f) are the two rotation angles; 2 and s identify the SONIC2 and SONANA instruments, respectively.

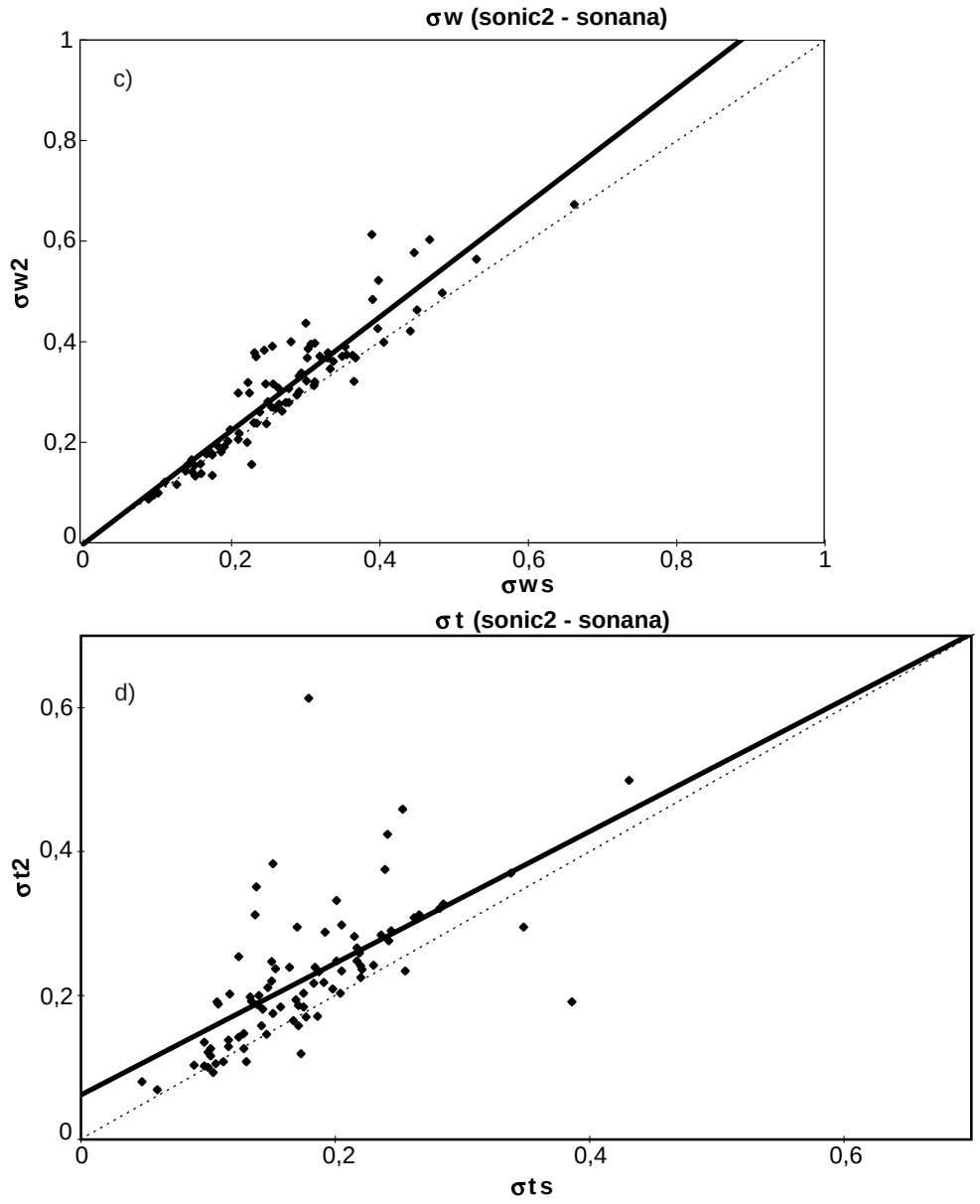

Fig. 10. – *Continued*.

However, the average sensible-heat flux observed in our experiment is of the same order of magnitude of the climatic daily trend quoted by [13], referring to a deeper region of Pacific Ocean off-shore of South Australia and showing an almost constant value of about -10 W/m^2 during daytime, with a minimum of about -20 W/m^2 at night.

To obtain more quantitative comparison, we present scatter diagrams between a few types of sampled or calculated quantities averaged over 30′. Figures 9 and 10 show

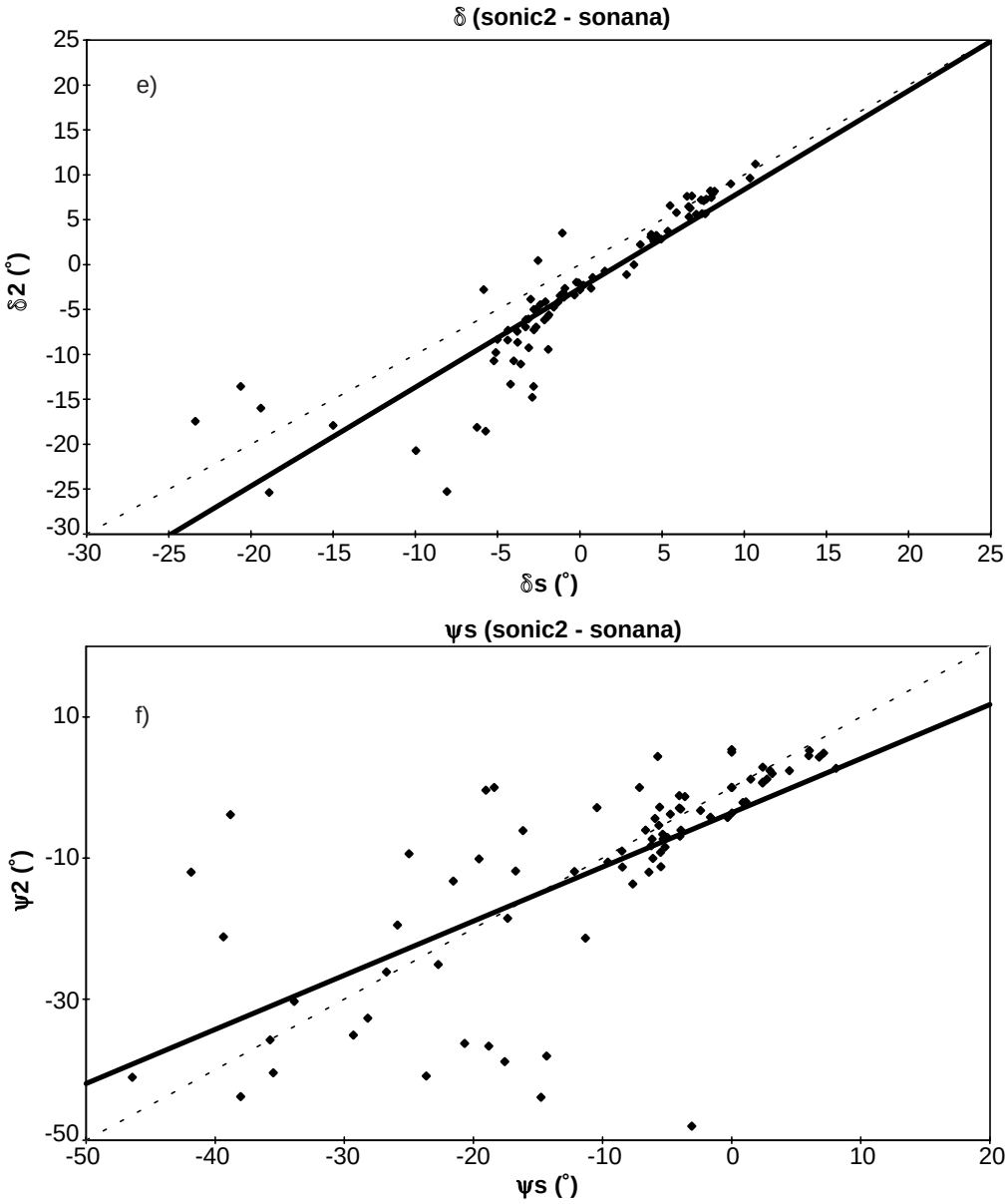

Fig. 10. – *Continued*.

some averaged quantities from different couples of instruments (SONIC1 *vs.* SONANA and SONIC2 *vs.* SONANA). For the other ones, the results are not significantly different; in table I and II the linear-correlation coefficients for all examined cases are listed.

As expected, better correlations are observed in general for data recorded by fast instruments at the same height (table II and III); in particular, fig. 9a) to d) shows that averaged horizontal wind speed and “sonic” temperatures are in more than

TABLE II. – *Linear-correlation coefficients r between average quantities calculated from ultrasonic anemometer data.*

r	Horizontal speed	Vertical speed	Sonic temperature	Wind direction	Friction velocity	Sensible heat flux
SONIC1-SONIC2	0.968	0.891	0.989	0.993	0.431	0.556
SONIC1-SONANA	0.968	0.936	0.987	0.996	0.541	0.443
SONIC2-SONANA	0.961	0.959	0.968	0.998	0.485	0.389
SONIC3-SONANA	0.912	−0.385	0.970	0.995	0.372	0.390
SONIC3-Kaijo Denki	0.631	0.650	0.979	0.738	0.601	0.319
SONIC1-SONIC3	0.896	−0.198	0.984	0.997	0.546	0.409
SONIC2-SONIC3	0.851	−0.538	0.987	0.994	0.398	0.013

TABLE III. – *Linear-correlation coefficients r between standard deviations σ and angle rotations ψ and δ calculated from ultrasonic anemometer data.*

r	σ_u	σ_v	σ_w	σ_t	δ	ψ
SONIC1-SONIC2	0.924	0.700	0.933	0.749	0.861	0.821
SONIC1-SONANA	0.927	0.740	0.941	0.664	0.921	0.856
SONIC2-SONANA	0.921	0.943	0.922	0.648	0.891	0.661
SONIC3-SONANA	0.584	0.688	0.405	0.560	−0.330	0.183
SONIC3-Kaijo Denki	0.571	0.531	0.912	0.388	0.501	−0.146
SONIC1-SONIC3	0.584	0.931	0.450	0.541	−0.140	0.106
SONIC2-SONIC3	0.475	0.622	0.395	0.472	−0.463	−0.117

satisfactory agreement with each other while other quantities, such as vertical wind component, friction velocities, “sonic sensible” fluxes variance, second-order crossed moments, and rotation angles, are more scattered (see fig. 9 e) and f), 10a) to f)).

Scatter diagram of data recorded at different heights (fig. 11a), evidences that the horizontal wind speeds are still in good agreement, but the vertical velocity (and, consequently, the rotation angles of the sonic reference system) show significant differences (fig. 11b), largely exceeding the ones observed for data measured at the same level, indicating higher sensitivity of these last quantities on their position relative to the platform. Also other second-order crossed moments involving vertical velocity fluctuations exhibit similar differences (fig. 11e) and f)), while sonic temperature and wind direction data seem to agree more satisfactorily with each other (fig. 11c) and d)). The last results could be a consequence of vertical turbulent eddies, induced by the platform when the wind impinges on it, whose size and strength could be different at various levels over the sea surface.

Airflow perturbation changes with height, thus it is not surprising that the vertical speeds are not correlated, being they larger in absolute value at lower level (this is not necessarily true if data considered are measured in different positions with respect to the obstacle’s axis). Moreover, remember that SONIC3 is shadowed by SITEP3 for ESE flows, that additional perturbations could result from border effects due to the limited lateral extension of the platform and that also the lack of a perfect alignment should affect the correlations.

From tables II and III it is possible to elicit that, setting the significant level to 5%, and being the number of data variable between 63 and 84, all quantities are satisfactorily correlated with each other in all examined cases, with the exclusion of the following cases:

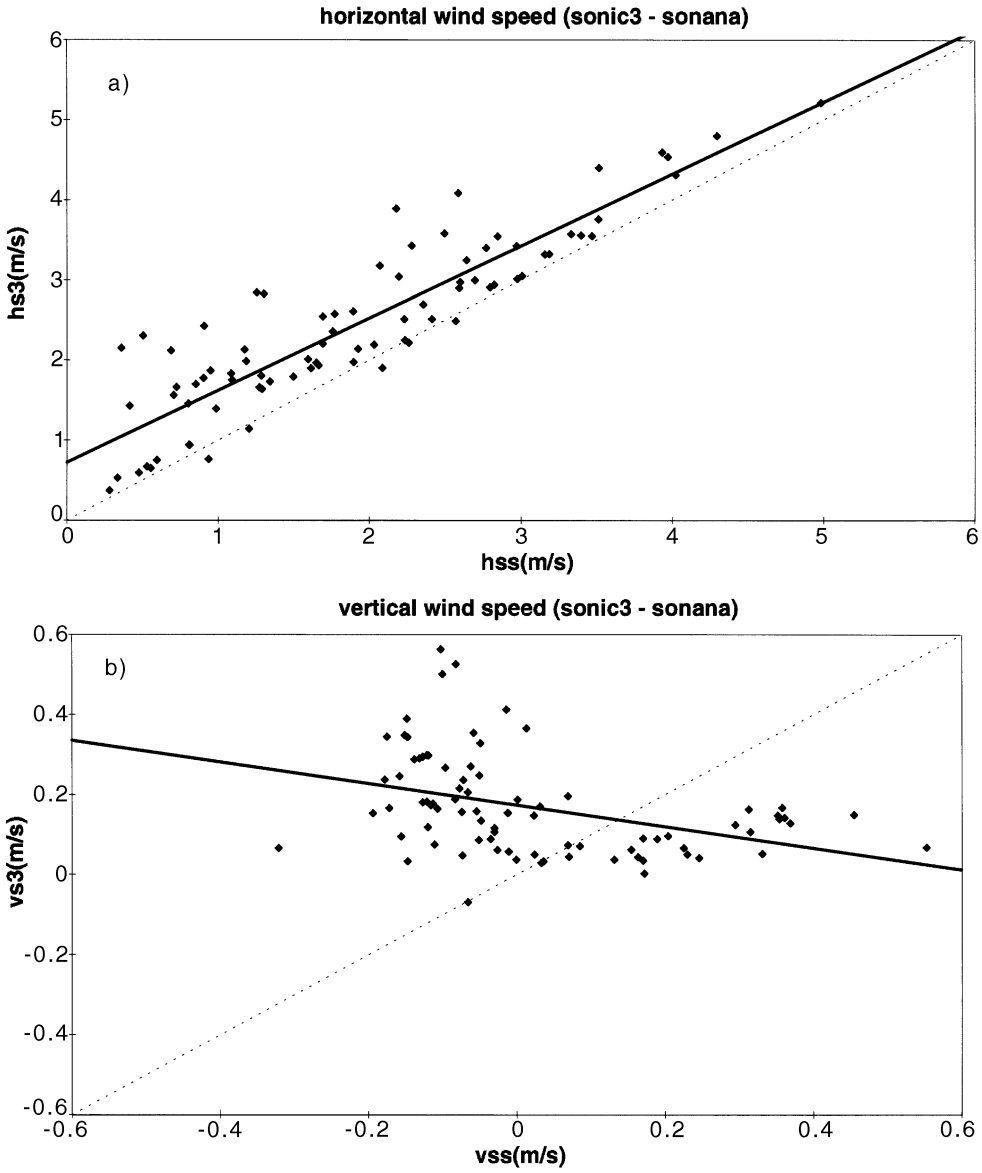

Fig. 11. – SONIC3 SONANA scatter diagrams: hs (a), vs (b), t (c), d (d), u* (e), and sf (f) are, respectively, the horizontal speed, vertical speed, sonic temperature, wind direction, friction velocity and sensible-heat flux measured by or calculated from ultrasonic anemometers; 3 and s indentify the SONIC3 and SONANA instruments, respectively.

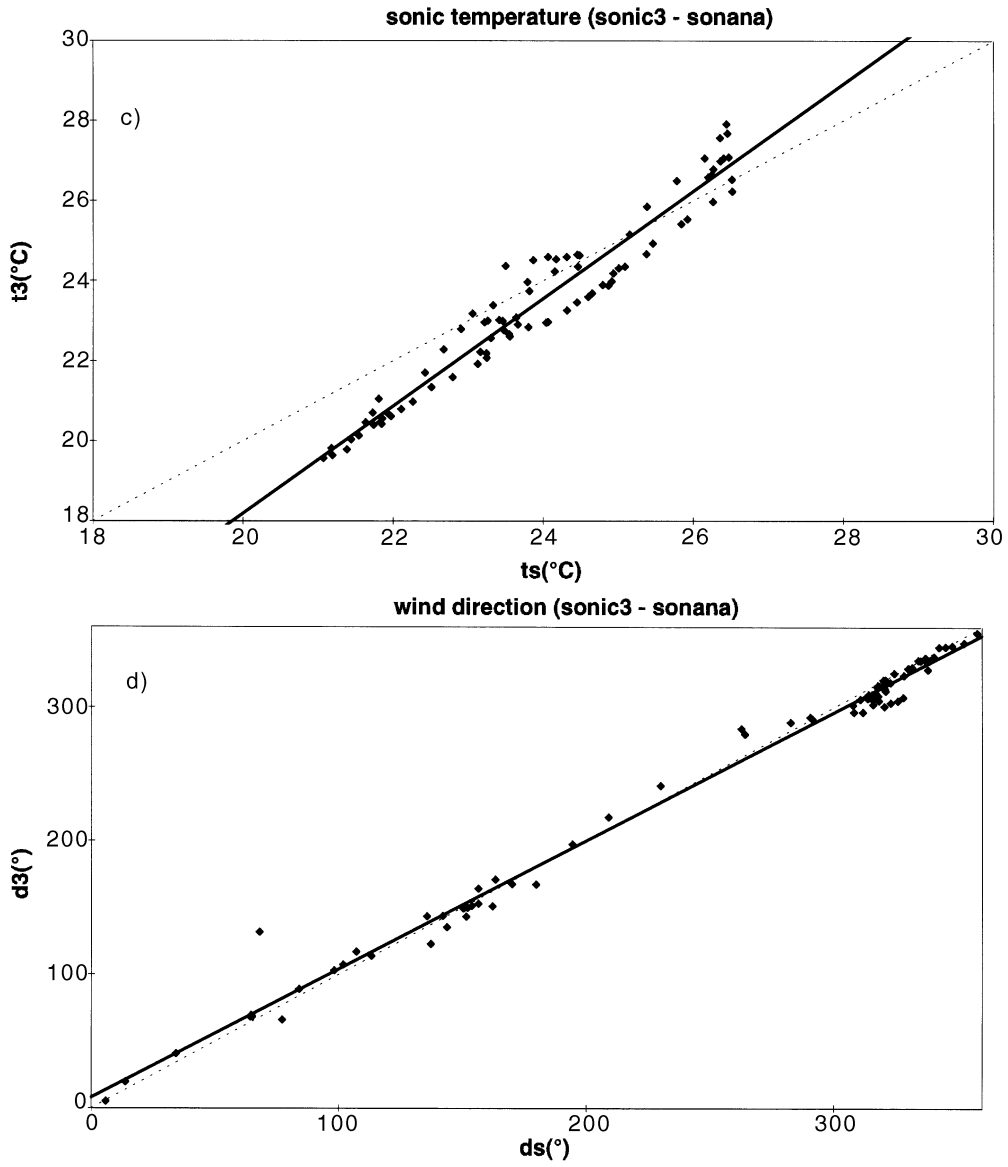

Fig. 11. – *Continued*.

a) SONIC1-SONIC3 for the vertical speed. This failure is plausible, because of the different height at which the instruments are located;

b) SONIC2-SONIC3 for the sensible-heat flux. The reason is the same as in the previous case.

c) SONIC3-SONANA, SONIC1-SONIC3, SONIC1-SONIC2, for the rotation angle ψ and SONIC1-SONIC3 for both ψ and δ. In this case too, these failures are due to the different instrument position.

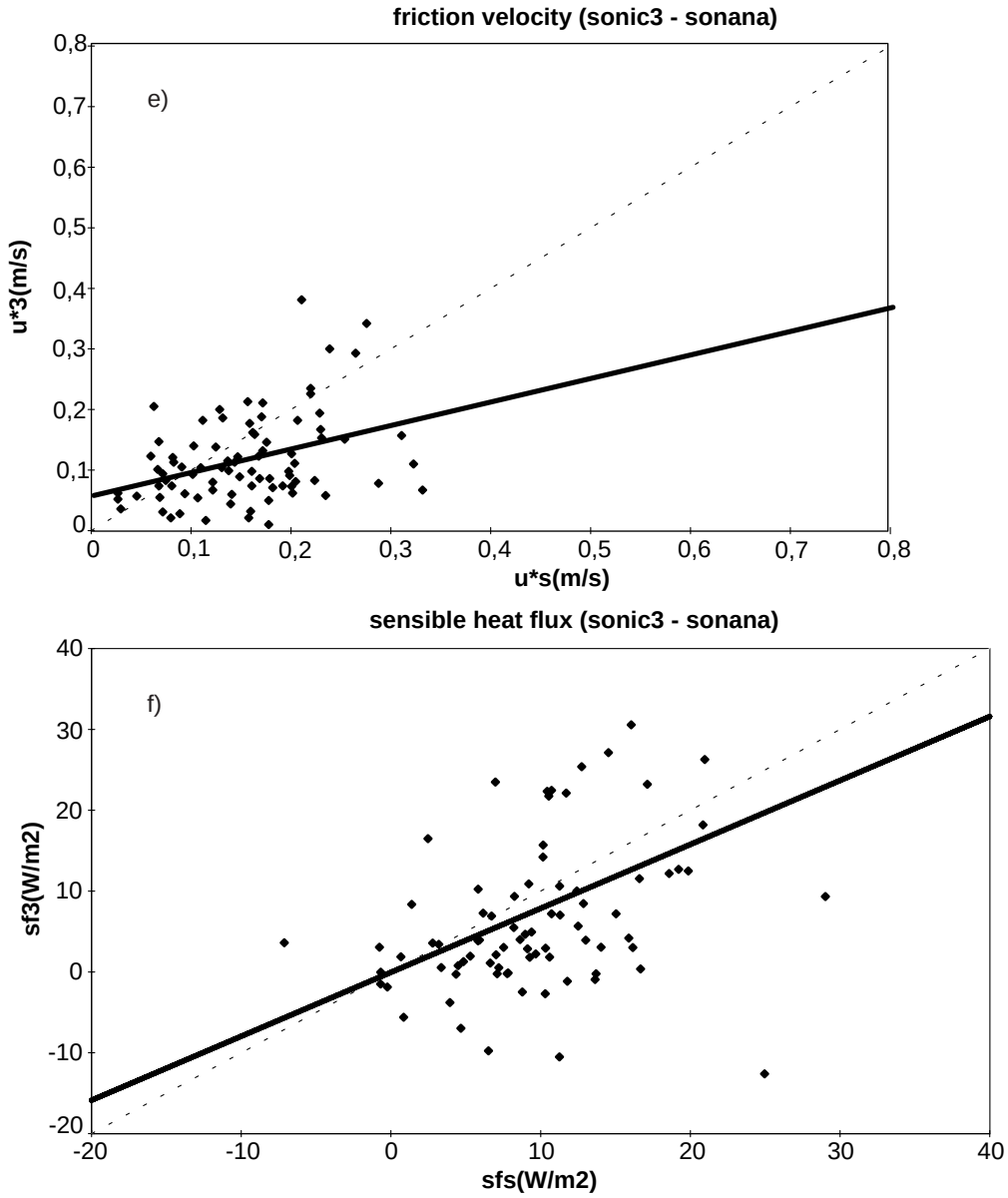

Fig. 11. – *Continued*.

d) SONIC3-Kaijo Denki for the sensible-heat flux and the angle ψ. This failure is probably to be ascribed to the different instrument performances, in addition to shadowing effects on SONIC3.

As to the comparison between "sonic" and absolute temperatures (respectively measured by the sonic anemometers and by the slow-response SITEP thermometers),

its results is shown in fig. 12, while in table IV the linear-correlation coefficients relative a set of 75 data are reported; it is possible to observe that in this case too we have obtained a satisfactorily good agreement.

At last, wind speeds and wind directions measured by sonic and traditional

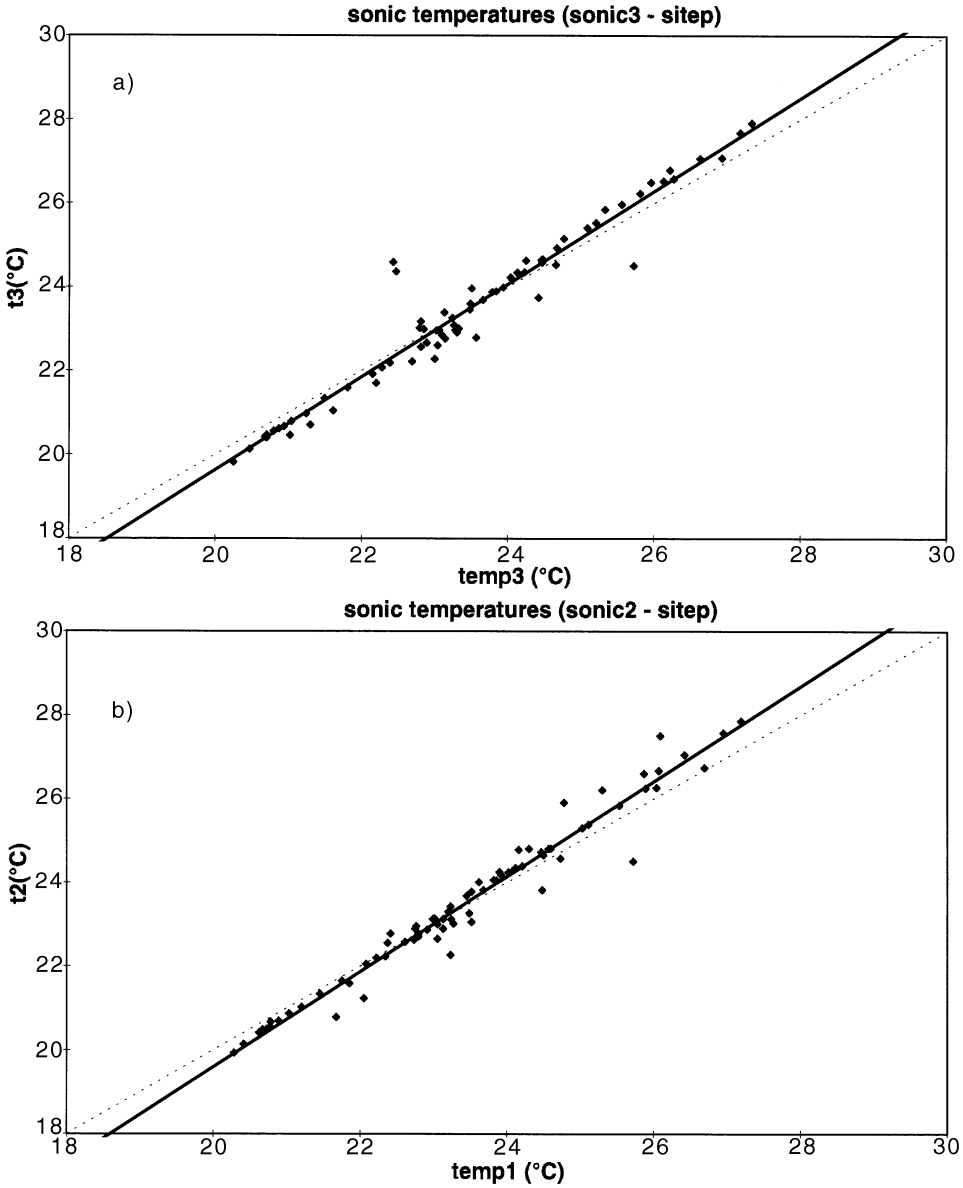

Fig. 12. – Temperature scatter diagrams: $t3$ (a), $t2$ (b), $t1$ (c), ts (d) (°C) are the temperatures computed from the ultrasonic anemometers SONIC3, SONIC2, SONIC1 and SONANA, respectively; temp1 and temp3 (°C) are the temperatures measured by the SITEP thermometers at 5 m and 10 m a.s.l., respectively.

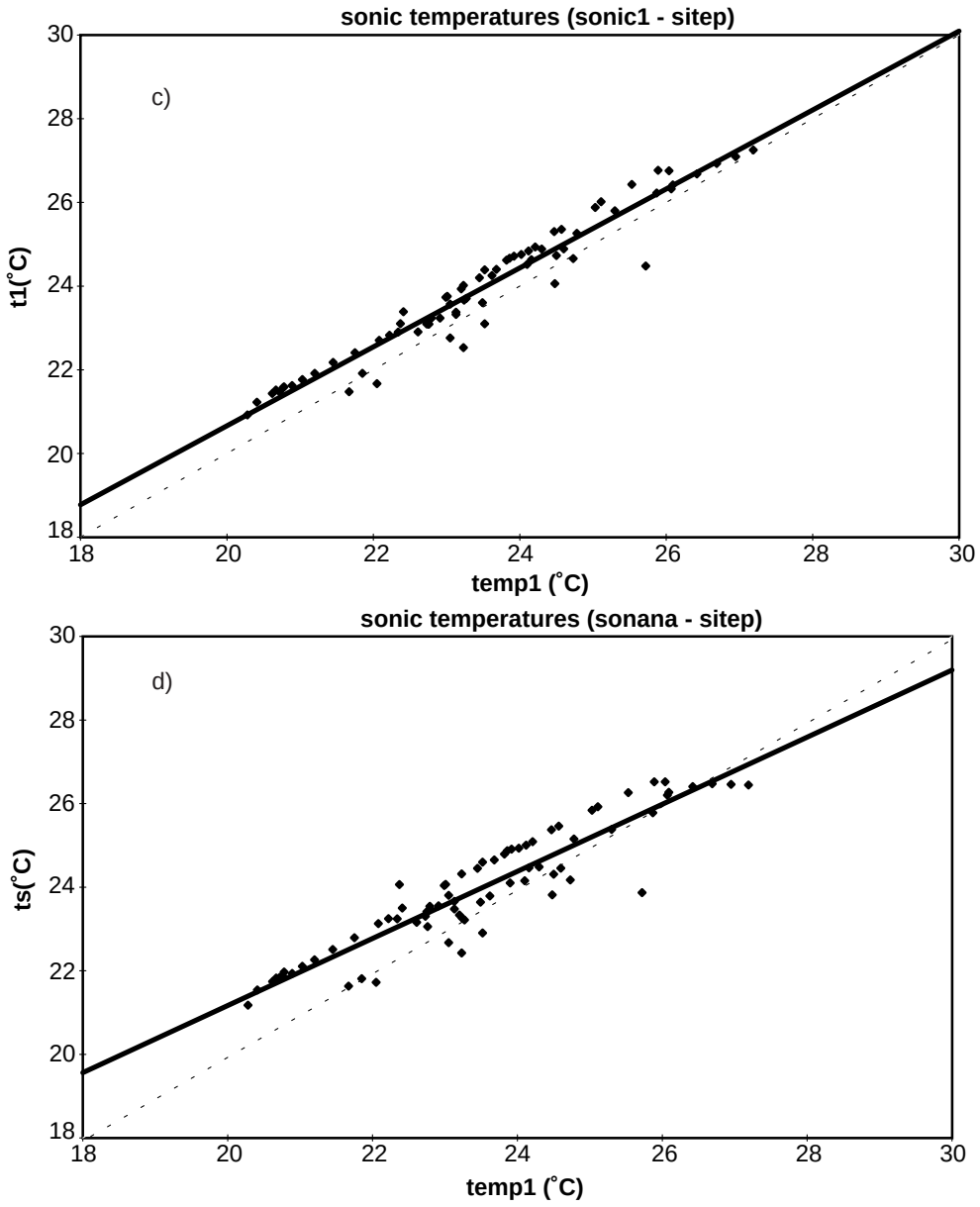

Fig. 12. – *Continued*.

anemometers have been compared with each other (fig. 13a) to d) and 14a) to d)). In table IV the linear-correlation coefficients relative to 66 data are reported. In this case it is possible to conclude that there is a greater, even if not important, disagreement among the data, which confirms the qualitative results of fig. 7 a) to d).

6. – Conclusions

The previous sections of this paper described an experimental campaign, carried out in June 1994 near Lerici (La Spezia, Italy) with the aim of studying the performance of

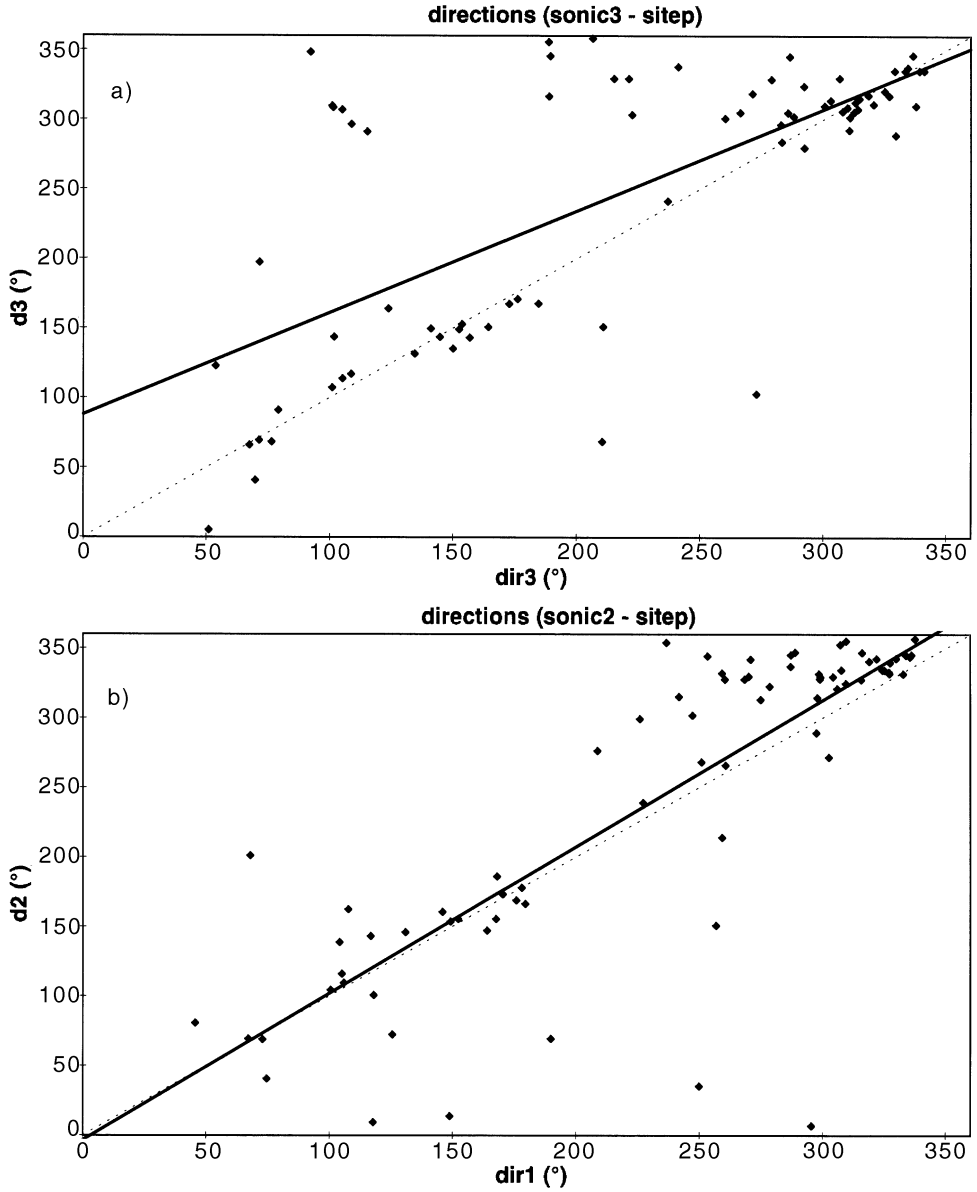

Fig. 13. – Direction scatter diagram: $d3$ (a), $d2$ (b), $d1$ (c) and ds (d) (degrees) are the wind directions recorded, respectively, by SONIC3, SONIC2, SONIC1 and SONANA; dir1 and dir3 (degrees) are the wind direction measured by the SITEP anemometres at the height of 5 m, and 10 m a.s.l., respectively.

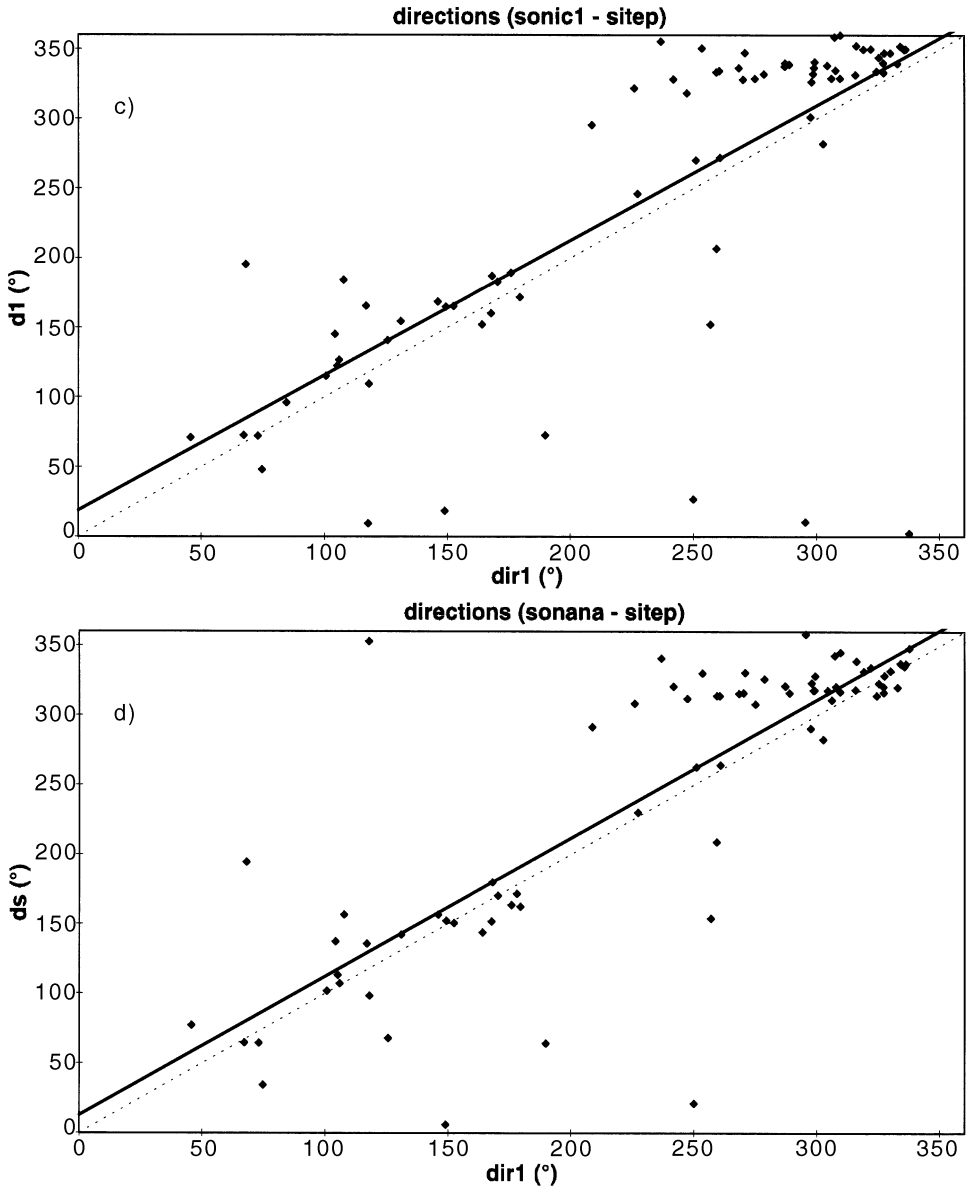

Fig. 13. – *Continued*.

instruments typically used for the assessment of surface energy exchange between sea and atmosphere. For this purpose, both fast instruments (5 ultrasonic anemometers and 1 fluxmeter) and low-response ones (3 anemometers, 1 barometer, 1 solarimeter, 4 thermometers and 3 hygrometers), set up on a mast at different heights below and above sea level (− 1 m, 2.5 m, 4 m, 7.5 m and 10 m), have been used.

Then, the values of measured and computed quantities from different instruments have been compared.

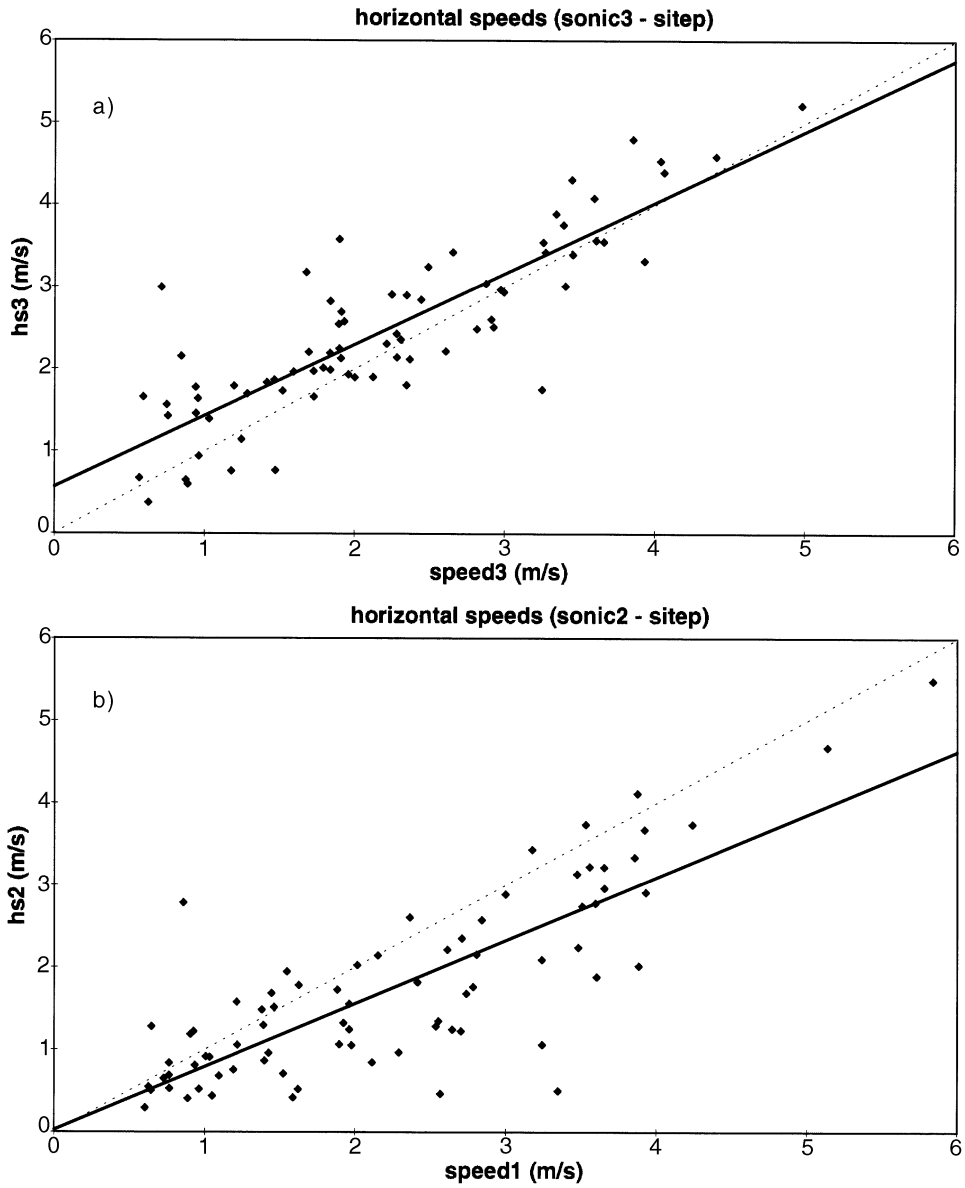

Fig. 14. – Speed scatter diagram: hs3 (a), hs2 (b), hs1 (c) and hss (d) (m/s) are the horizontal wind speeds recorded by SONIC3, SONIC2, SONIC1 and SONANA, respectively. speed1 and speed3 (m/s) are the two horizontal wind speeds measured by the SITEP anemometres at the height of 5 m, and 10 m a.s.l., respectively.

Traditional and fast instruments (as far as average quantities were concerned) have shown satisfactory and reasonable agreement with each other even if they were located at different heights.

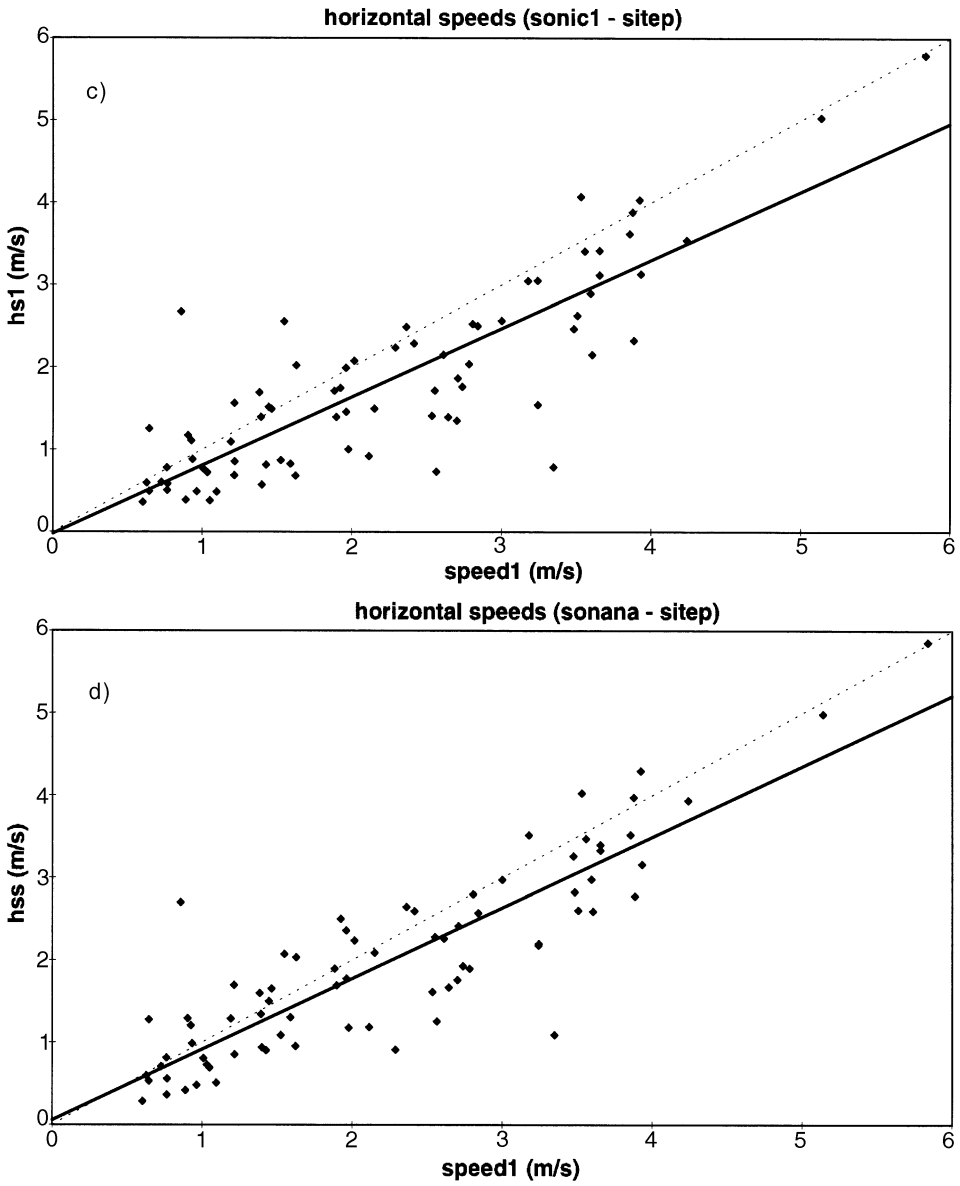

Fig. 14. – *Continued*.

Fast-response instruments of the same type and manufacturer, indeed provided measures of horizontal wind speed and direction, and sonic temperature, which were in good agreement, with a meaningful correlation degree (from 0.85 to 0.97 at a significant level of 5%) which was higher for quantitities sampled at the same height.

Vertical wind speeds too appeared to be satisfactorily correlated with each other when they were measured at the same height by instruments of the same type and

TABLE IV. – *Linear-correlation coefficients r between sonic temperatures, wind direction and horizontal wind speed calculated from ultrasonic and conventional anemometers data.*

r	SONIC3-SITEP3	SONIC2-SITEP1	SONIC1-SITEP1	SONANA-SITEP1
sonic temperature	0.972	0.982	0.969	0.928
wind direction	0.696	0.823	0.747	0.823
wind speed	0.853	0.813	0.851	0.879

manufacturer and still exhibited moderate correlation when they were measured by different instruments at the same height, but their correlation degree dropped to very low values when they were measured at different heights, even by similar instruments.

This behaviour has repercussions on the correlation degree of second-order crossed moments involving vertical speed fluctuation (like friction velocity and sensible-heat flux) whose correlation coefficient, in this experiment, could can hardly exceed 0.6, at a significance lavel of 5%.

The above results point out that flow disturbances induced on the airflow by obstacles like a marine platform are mainly reflected on the vertical component of the turbulent wind speed and, as a consequence, on the vertical fluxes of atmospheric properties when these last are evaluated through the eddy correlation method.

* * *

The authors are grateful to Dr. MELONI (Stazione Oceanografica CNR S. Teresa), Mr. BELARDINELLI (CNR -IFA) and Messrs. MANZI and QUINTERI (ENEL-CRAM) for the technical assistance during the campaign, and to the PNRA for its partial financial support.

APPENDIX A

Fast-response sensors:

a) Solent ultrasonic anemometers

This anemometer consists of a sensing head with six ultrasonic transducers arranged in three pairs. The transducers axes are all oriented at 45° with respect to the vertical direction. Furthermore, their projections on the horizontal plane are at 120°, with the first transducer 30° anticlockwise from the north direction. Each pair of transducers acts alternately as transmitter and receiver, sending back and forth high-frequency ultrasound pulses. The software provided by the Gill Instruments [14] allows to calculate and store, ~ 21 times per second, the wind velocities along the three axes u, v, w and the sound volocity c (each with an accuracy of 1.5%), and also allows to correct and calibrate the three vector speeds taking into account the effects of the framework and transducers.

b) Kaijo Denki ultrasonic anemometer

This is another type of fast-response anemometer, with quite a different structure from the previous one: its 6 sensors are fixed two by two on 3 axes, one vertical and the other two lying at 120° on the same plane perpendicular to the first axis. The software

provided by Kaijo Denki gives in output the 3 components of wind speed in an orthogonal system and the sonic temperature, at a sampling rate of 20 Hz; the wind speed accuracy is about 1% [15].

c) Campbell sensible heat fluxmeter

This fluxmeter is made up by one vertical ultrasonic anemometer and one fast sensor gauging the air temperature. The vertical fluctuations of the wind are measured continuously by the ultrasonic anemometer, model CA27, designed by Campbell and Unsworth in 1979 [16]; the width between the two sensors is equal to 10 cm. The CA27 sonic anemometer is a fast-response single-axis instrument producing accurate and reliable measurements of the rapid fluctuations of wind speed in typical conditions of a turbulent atmosphere. The temperature fluctuations are measured by the Fast Response Thermocouple (model 127).

Slow-response sensors:

a) The wind sensor SITEP ML-7327 is built according to solid-state technology and has no revolving parts. The working principle is based upon the transduction of the force exerted by wind on a cylindrical surface; this force is then split into the two orthogonal components on the horizontal plane. The instrument samples the wind direction (degrees) and speed (knots) at a frequency of 4 Hz with an accuracy of, respectively, $\pm 3°$ and ± 1 knot.

b) The sensor of solar radiation is made by a solar silicon cell. The sampling frequency is 10^{-2} Hz.

c) The sensors of pressure, temperature and humidity are conventional instruments on the market, they have sampling of frequencies 10^{-2} Hz.

REFERENCES

[1] HASTENRATH S. and LAMB P. J., *On the heat budget of hydrosphere and atmosphere in the Indian Ocean, J. Phys. Oceanogr.,* **10** (1980) 694-70.
[2] MEYERS G., DONGUY J. R. and REED R. K., *Evaporative cooling of the Western Equatorial Pacific Ocean during 1892-83*, *Nature* (*London*), **312** (1986) 258-260.
[3] MOLINARI R. L. and HAUSEN D. V., *Observational studies of near surface thermal budgets in the tropics,* in *Further Progress in Equatorial Oceanography*, edited by E. KATZ and J. WITTE (Nova University Press, Fort Lauderdale, Fla).
[4] NIILER P. and STEVENSON J., *The heat budget of Tropical Ocean warm water pools*, *J. Mar. Res.,* **40** (1982) 465-480.
[5] SCHOPF P. S. and CANE M. A., *On Equatorial dynamics, mixed layer phyics and sea surface temperature, J. Phys. Oceanogr.,* **13** (1983) 917-935.
[6] STEVENSON J. W. and NIILER P. P., *Upper ocean heat budget during the Hawaii-to-Tahiti Shuttle Experiment, J. Phys Oceanogr.,* **13** (1983) 1894-1907.
[7] BLANC T. V., *Variation of bulk-derived surface flux, stability and roughness results due to the use of different transfer coefficient schemes, J. Phys. Oceanogr.,* **15** (1985) 650-669.
[8] ARYA S. P., *Introduction to Micrometeorology* (Academic Press Inc.) 1988.
[9] CASSARDO C, SACCHETTI D., MORSELLI M. G., ANFOSSI D., BRUSASCA G. and LONGHETTO A., *A study of the assessment of air temperature, and sensible- and latent-heat fluxes from sonic-anemometer observation, Nuovo Cimento C,* **18** (1995) 419.

[10] MC MILLEN R. T., *An eddy correlation technique with extended applicability to non-simple terrain, Boundary-Layer Meteorology,* **43** (1988) 231-345.
[11] ANFOSSI D., CASSARDO C., FERRERO E., LONGHETTO A., SACCHETTI D., BRUSASCA G., COLOMBO V., MARZORATI A., MORSELLI M. G., ROCCHETTI F. and TINARELLI G., *On the analysis of ultrasonic anemometer data,* Internal Report No. 282/93 of Istituto di Cosmogeofisica, CNR (National Research Council) 1993.
[12] PIELKE R. A., *Mesoscale Meteorological Modelling* (Academic Press Inc.,) 1984.
[13] VAN LOON H., *Climates of the Oceans, World Survey of Climatology*, edited by H. E. LANDSBERG, Vol. **15** (Elsevier) 1984, pp. 343-344.
[14] GILL G. C., *Solent research ultrasonic anemometer product specifications Issue 4.1*, Gill anemometer reference user's guide (Gill Instruments Ltd.) 1992.
[15] KAIJO DENKI, *Digitized ultrasonic anemometer thermometer model DAT-300,* Instruction manual (Kaijo Denki Co. Ltd., Tokyo) 1982.
[16] CAMPBELL G. S. and UNSWORTH M. H., *An inexpensive sonic anomometer for eddy correlation, J. Appl. Meteorol.*, **18** (1979) 1072-1077.